

# Structure, folding and flexibility of co-transcriptional RNA origami

---

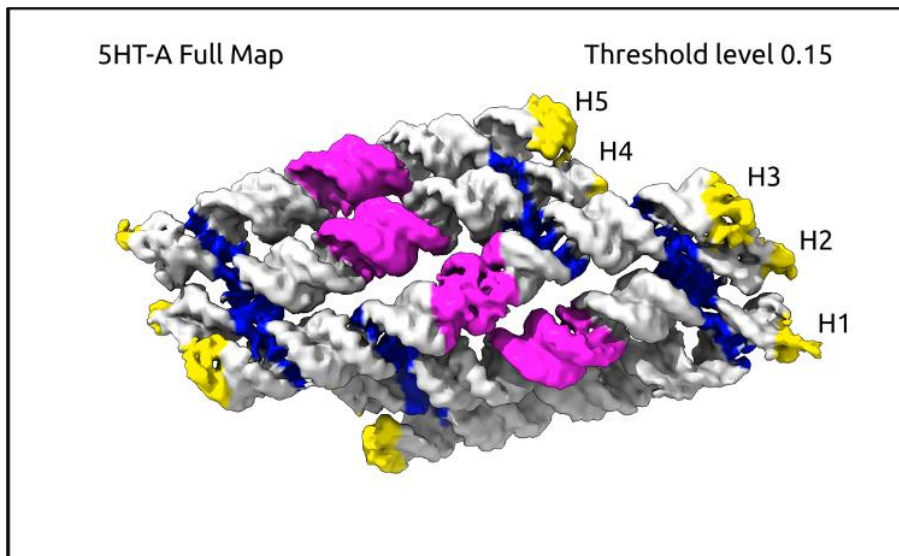
In the format provided by the authors and unedited

## Content:

Supplementary Video 1. Cryo-EM reconstruction of the 5HT-A RNA origami.....	3
Supplementary Video 2. 6HBC maturation necessitates the breaking of the H6 KL.....	3
Supplementary Video 3. Local dynamics of the 5HT-A RNA origami. ....	4
Supplementary Video 4. Local dynamics of the 6HBC Young and Mature conformers. ....	4
Supplementary Table 1. RNA sequence and blueprint for 5-helix tile A (5HT-A).....	5
Supplementary Table 2. RNA sequence and blueprint for 5-helix tile A with twist correction (5HT-A-TC).....	6
Supplementary Table 3. RNA sequence and blueprint for 5-helix tile B (5HT-B). ....	7
Supplementary Table 4. RNA sequence and blueprint for 5-helix tile B (5HT-B-V2).....	8
Supplementary Table 5. RNA sequence and blueprint for 5-helix tile B with 3 KL columns (5HT-B-3X). ....	9
Supplementary Table 6. RNA sequence and blueprint for 6-helix bundle (6HB).....	10
Supplementary Table 7. RNA sequence and blueprint for 6-helix bundle with clasp (6HBC). ....	11
Supplementary Table 8. RNA sequence and blueprint for 6-helix bundle with clasp and protein binding sites (6HBC-PBS).....	12
Supplementary Table 9. RNA sequence and blueprint for 16-helix satellite (6HS).....	13
Supplementary Table 10. Cryo-EM data collection, refinement and validation statistics.....	14
Supplementary Table 11. Seam curvature angles $\phi$ measured from 3DVA of 5HT-A. ....	15
Supplementary Table 12. Crossover angles $\theta$ measured from 3DVA of 5HT-A. ....	17
Supplementary Fig. 1. Cryo-EM data and reconstruction of 5HT-A. ....	19
Supplementary Fig. 2. Cryo-EM data and reconstruction of 5HT-A-TC. ....	20
Supplementary Fig. 3. Cryo-EM data and reconstruction of 5HT-B.....	21
Supplementary Fig. 4. Cryo-EM data and reconstruction of 5HT-B-3X. ....	22
Supplementary Fig. 5. Cryo-EM data and reconstruction of 6HB. ....	23
Supplementary Fig. 6. Cryo-EM data and reconstruction of 6HBC-Young1.....	24
Supplementary Fig. 7. Cryo-EM data and reconstruction of 6HBC-PBS-Mature1. ....	25
Supplementary Fig. 8. Cryo-EM data and reconstruction of 6HBC-Young2.....	26
Supplementary Fig. 9. Cryo-EM data and reconstruction of 6HBC-Mature2.....	27
Supplementary Fig. 10. Map to model correlation of 5HT-A. ....	28
Supplementary Fig. 11. Map to model correlation of 5HT-A-TC.....	29
Supplementary Fig. 12. Map to model correlation of 5HT-B.....	30
Supplementary Fig. 13. Map to model correlation of 6HBC-Young1. ....	31
Supplementary Fig. 14. Map to model correlation of 6HBC-PBS-Mature1. ....	32
Supplementary Fig. 15. Cryo-EM 2D class averages of the 16H-satellite sample.....	33
Supplementary Fig. 16. IPET 3D reconstruction of individual particle #1 of 16HS.....	34

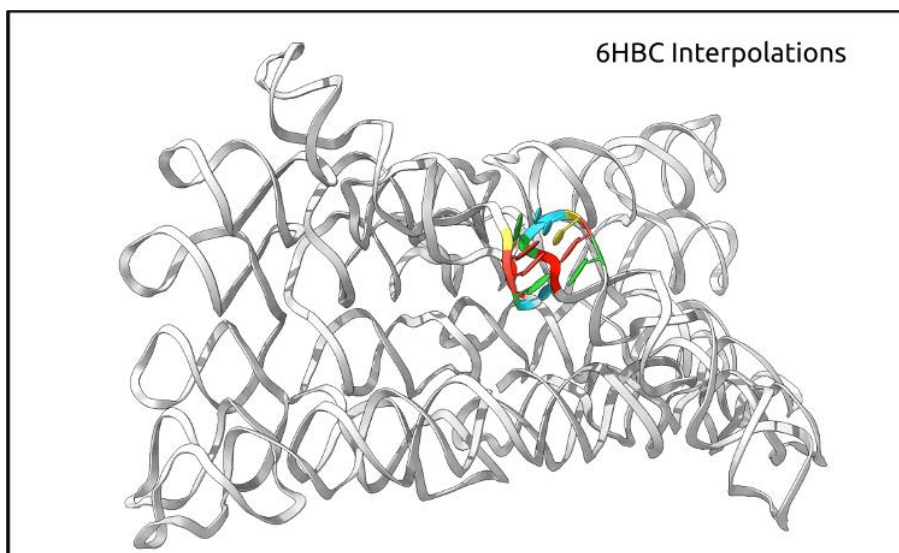
Supplementary Fig. 17. IPET 3D reconstruction of individual particle #2 of 16HS.....	35
Supplementary Fig. 18. IPET 3D reconstruction of individual particle #3 of 16HS.....	36
Supplementary Fig. 19. IPET 3D reconstruction of individual particle #4 of 16HS.....	37
Supplementary Fig. 20. IPET 3D reconstruction of individual particle #5 of 16HS.....	38
Supplementary Fig. 21. IPET 3D reconstruction of individual particle #6 of 16HS.....	39
Supplementary Fig. 22. IPET 3D reconstruction of individual particle #7 of 16HS.....	40
Supplementary Fig. 23. IPET 3D reconstruction of individual particle #8 of 16HS.....	41
Supplementary Fig. 24. IPET 3D reconstruction of individual particle #9 of 16HS.....	42
Supplementary Fig. 25. IPET 3D reconstruction of individual particle #10 of 16HS.....	43
Supplementary Fig. 26. IPET 3D reconstruction of individual particle #11 of 16HS.....	44
Supplementary Fig. 27. IPET 3D reconstruction of individual particle #12 of 16HS.....	45
Supplementary Fig. 28. IPET 3D reconstruction of individual particle #13 of 16HS.....	46
Supplementary Fig. 29. IPET 3D reconstruction of individual particle #14 of 16HS.....	47
Supplementary Fig. 30. IPET 3D reconstruction of individual particle #15 of 16HS.....	48
Supplementary Fig. 31. IPET 3D reconstruction of individual particle #16 of 16HS.....	49

## Legends and stills for supplementary videos



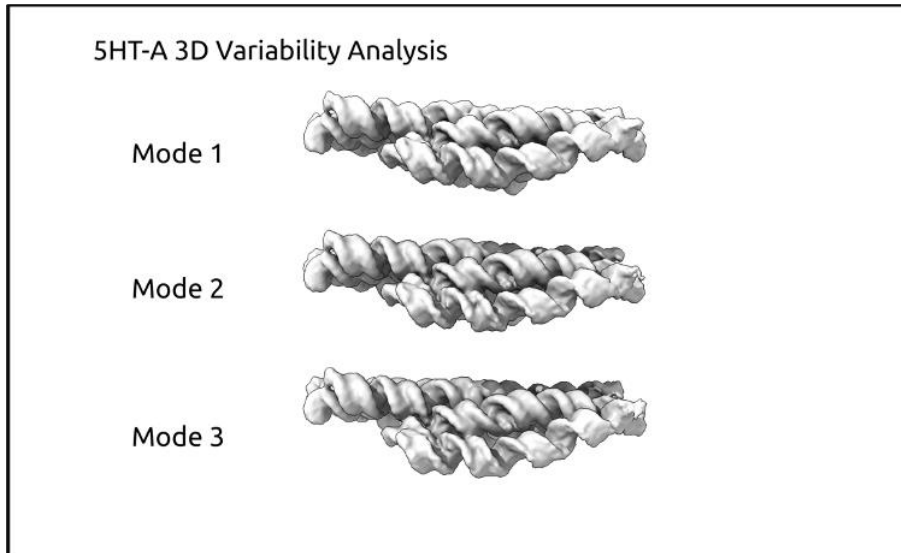
### Supplementary Video 1. Cryo-EM reconstruction of the 5HT-A RNA origami.

Depicted first is the map from a local refinement using a mask covering the entire structure, autogenerated by cryoSPARC. Coloring has been applied to the map through the motifs modeled into the map. Tetraloops are depicted in yellow, crossovers in blue and KLs in magenta. The map is further refined by local refinement using a mask covering only H2-H4 (shown in grey 0:47-0:51). This results in better local resolution at the crossovers and central KL. Local resolutions are colored on the map surface.



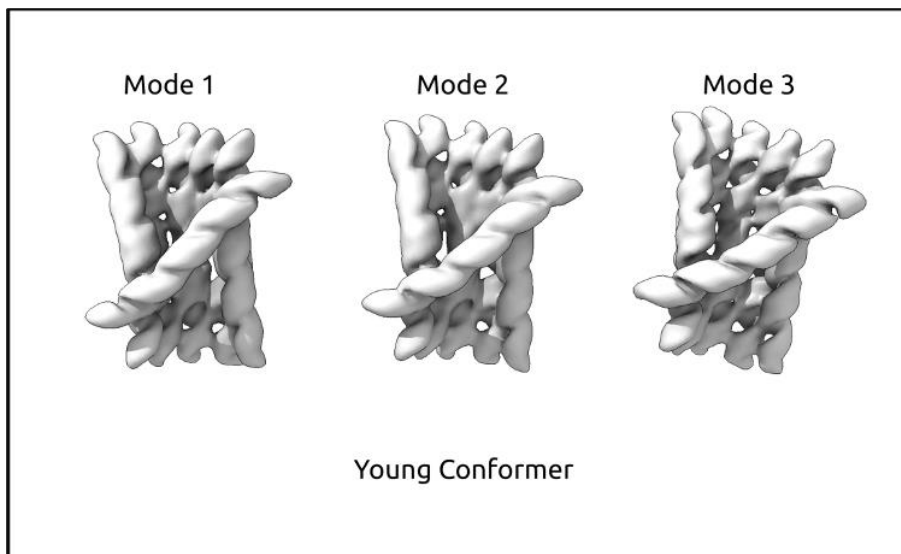
### Supplementary Video 2. 6HBC maturation necessitates the breaking of the H6 KL.

Depicted first are the reconstructions of the young and mature 6HBC conformers with the surface near the A2:A2' stack colored red. The A2:A2' stack of the young conformer faces inward but the A2:A2' stack of the mature conformer faces outward. Rotation of each half of H6 in opposite directions is required to transition between the two conformers, when visualized by interpolation it becomes clear that the central KL must break for this to occur.



**Supplementary Video 3. Local dynamics of the 5HT-A RNA origami.**

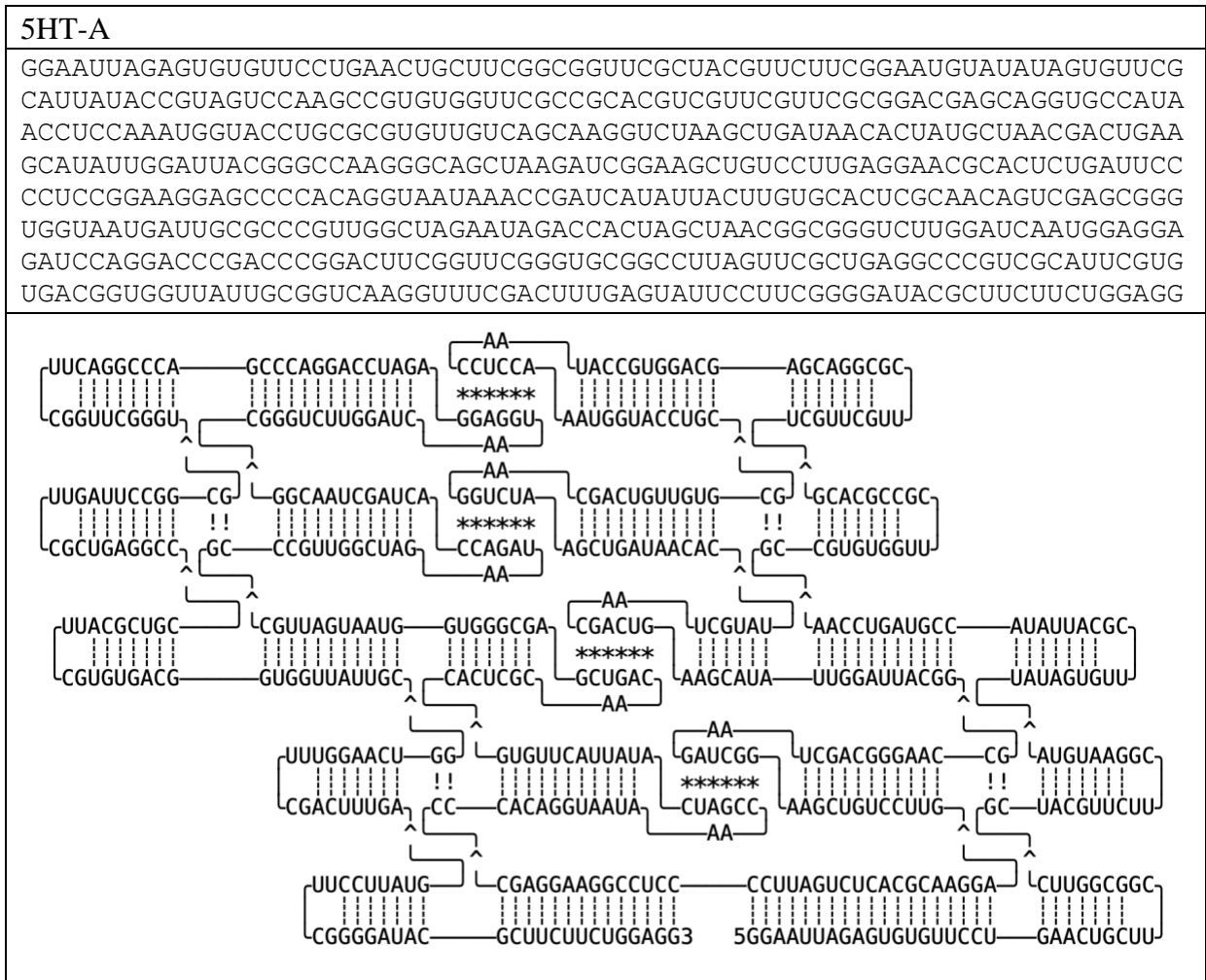
Three principal modes of variability were solved using cryoSPARC's 3D variability analysis algorithms. Each mode is displayed as a volume series comprised of 20 different volumes reconstructed from particle sets classified along a given motion trajectory.



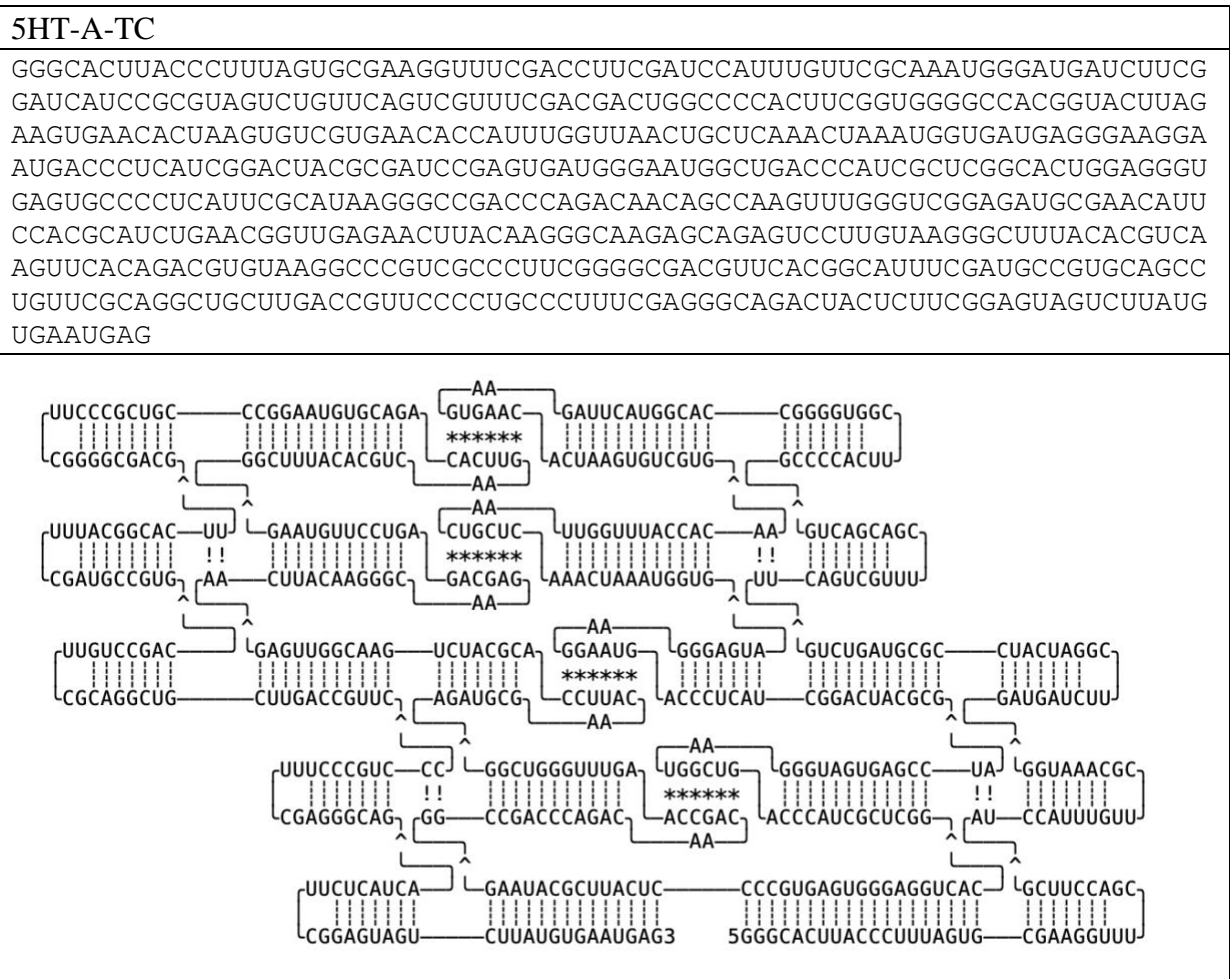
**Supplementary Video 4. Local dynamics of the 6HBC Young and Mature conformers.**

Three principal modes of variability were solved from both the 6HBC-Young and 6HBC-Mature datasets, using cryoSPARC's 3D variability analysis algorithms. Each mode is displayed as a volume series comprised of 20 different volumes reconstructed from particle sets classified along a given motion trajectory.

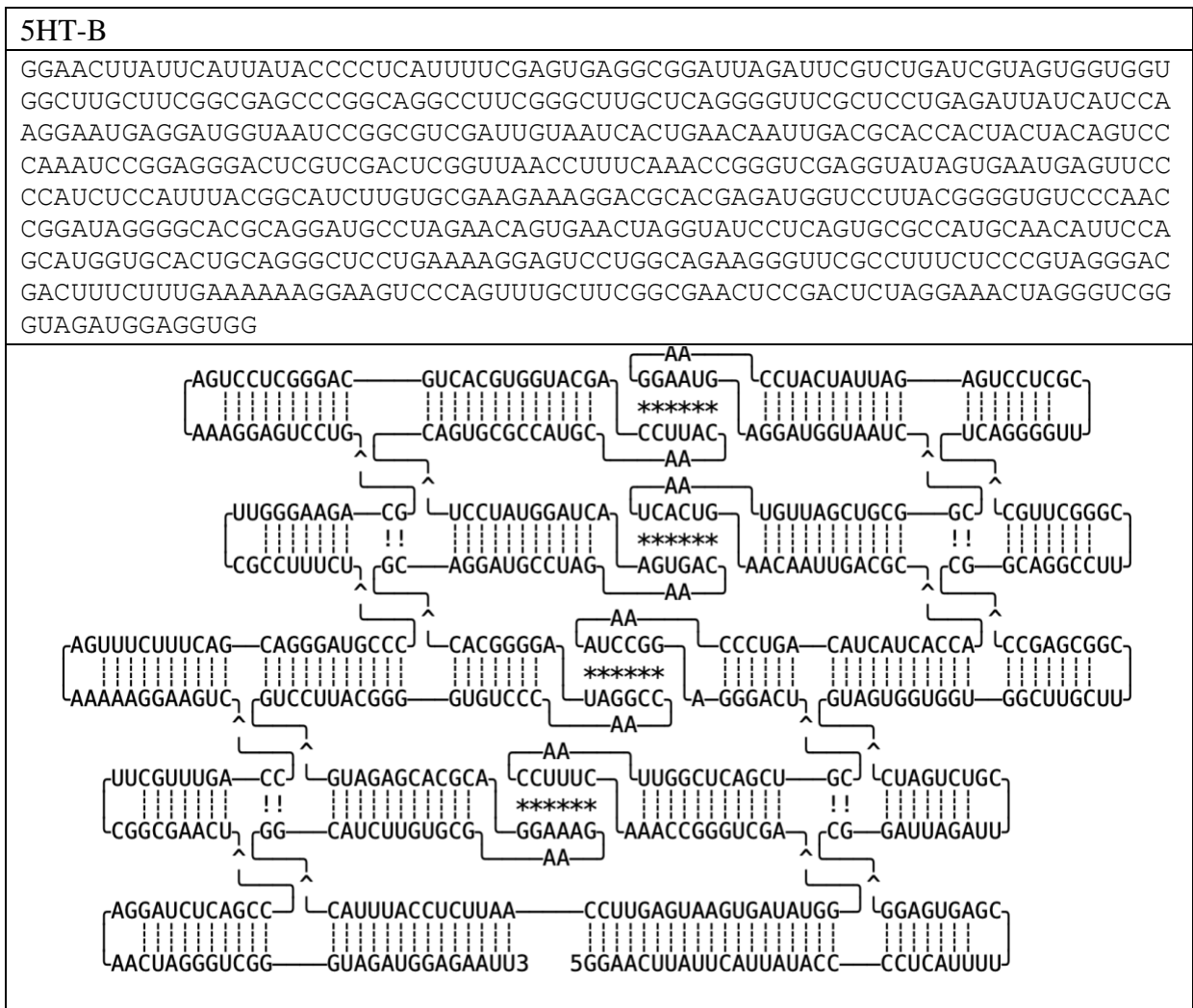
**Supplementary Table 1. RNA sequence and blueprint for 5-helix tile A (5HT-A).**



**Supplementary Table 2. RNA sequence and blueprint for 5-helix tile A with twist correction (5HT-A-TC).**

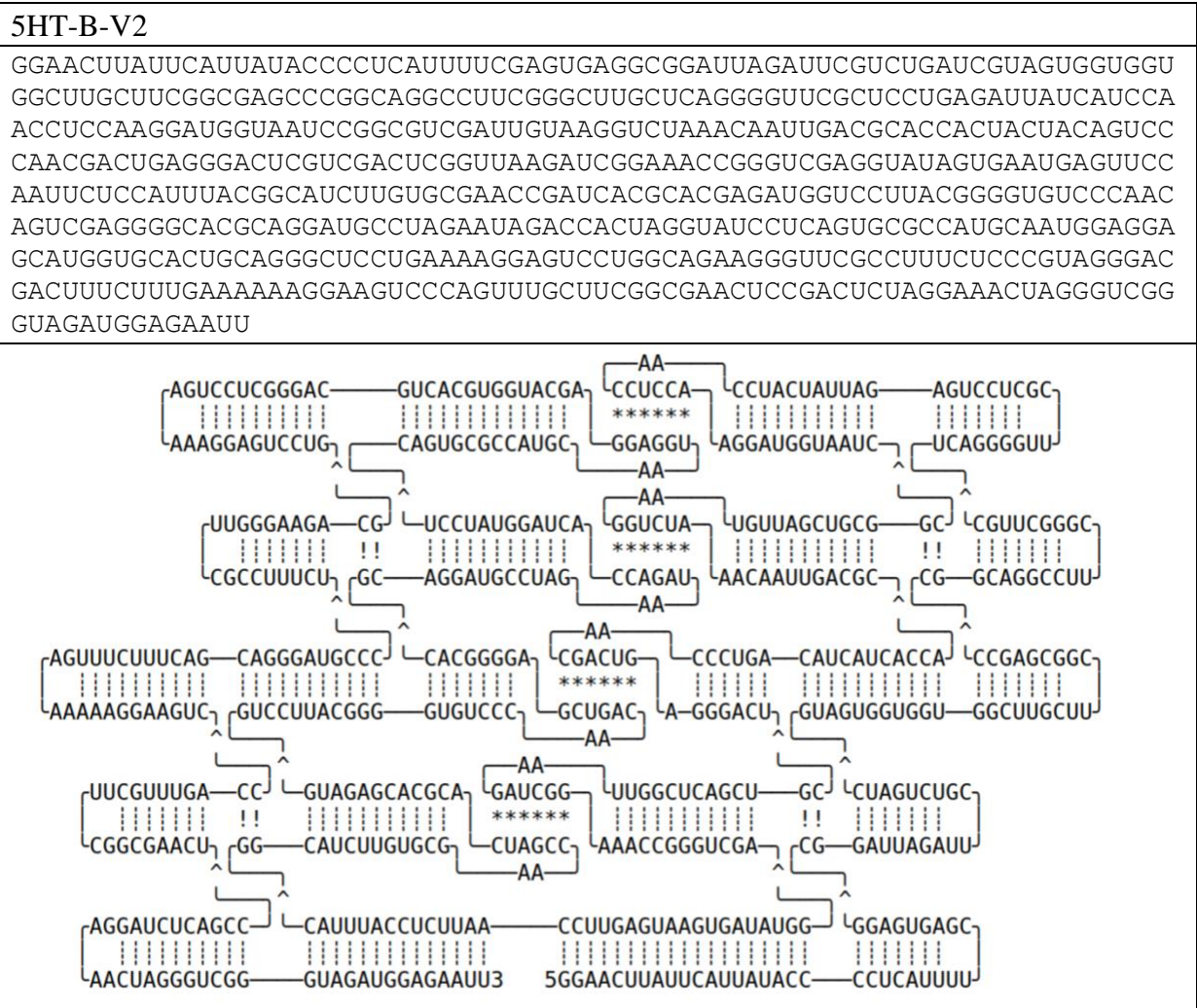


**Supplementary Table 3. RNA sequence and blueprint for 5-helix tile B (5HT-B).**

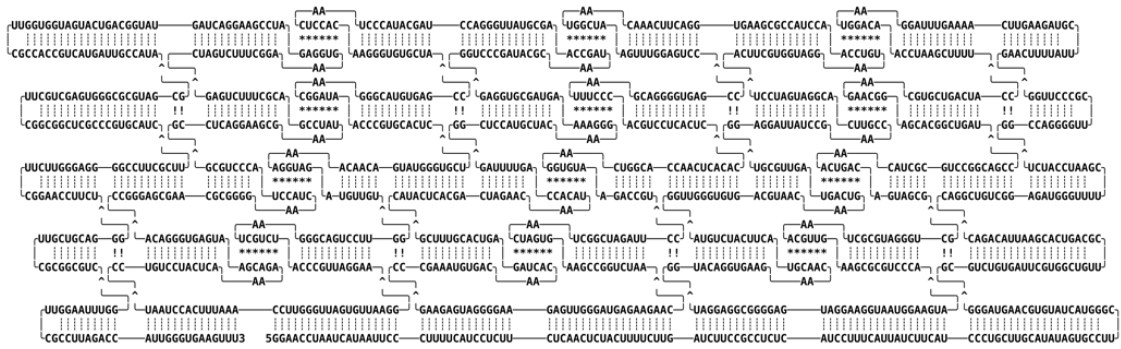




**Supplementary Table 4. RNA sequence and blueprint for 5-helix tile B (5HT-B-V2).**



**Supplementary Table 5. RNA sequence and blueprint for 5-helix tile B with 3 KL columns (5HT-B-3X).**

5HT-B-3X
<p>GGAACCUAAUCAUAAUUCUUUUUCAUCCUCUUCUCAACUCUACUUUUUCUUGAUCUUCGCCUCUCAU            CCUUUCAUUUAUCUUCUACUCCUGCUUGCAUAUAGUGCCUUCGGGUACUAUUGGCAAGUAGGGGCGUCUG            UGAUUCGUGGCUGUUCGCAGUCACGAAUACAGACCAGGCUGUCGGAGAUGGGUUUUUCGAAUCCAUCU            GGCCAGGGGUUCGCCUUUGGGAACUUUUUAUUCGUAGAAGUUCAAAAGUUUAGGAAUGGACAACCUAAG            CUUUUCCAUCAGUCGUGCAAGAACGGAGCACGGCUGAUCCGACGGCCUGCGCUACAAACUGACAGUAG            CGGCUGGGGAUGCGCUAAACGUUGAAGCGCGUCCCAAUGAAGGUAUUGGAAGGAUGAGGGGCGGAGGAU            GGUACAGGUGAAGAACAACGUACUUCUACUCUGUAGGUUGGGUGUGACGUAACAAGUCAGUAGUUGCGUG            GAGGAUUAUCCGAACCGUUCACGGAUGAUCCUACUUCGUGGUAGGAAUGUCCAACCUACCGCGAAGUG            GACUUCAAACAAGGCUAAGUUUGGAGUCCCGAGUGGGGACGAAUUUCCACGUCCUCACUCCACAC            UCAACCACGGUCAAGGUGUAAGACCGUCCUAGAUCCGCUAACUAGUGAAGCCGGUCUACAAGAAGA            GUAGGGUUGAGAAGGGGAUGAGAAGCCCGAAAUGUGACAACACUAGAGUCAGUUUCGCAUACUCACG            ACUAGAACAUAACACCAGUUUAGGGUCUCCAUGCUACAAGGGAAAAGUAGCGUGGAGGGUCCCGAUAC            GCAAUAGCCAAGCGUAUUGGGACCUAGCAUACCUAACUCCACAAGGGUGUGCUACCGAGUGUACGGG            AACGGUAUACCCGUGCACUCUCGUGGGUAUGACAACAAAAGGUAUGUUGUGGUUCCUGACGGGAAU            CGUCUACCCGUUAGGAAGGAAUUGUGAUUGGGUUCAAAUUUACCCUAAUCCUGUCCUACUAAAAGA            CGAAUGAGUGGGACACCGGGAGCGAACCGGGGAACUACCUACCCUGCGGCCUCAGGAAGCGAAUAUC            CGACGCUUUCUGAGCUAGUCUUUCGGAAGUGGAGAUCCGAAGGACUAGUAUGGCAGUCAUGAUGGUG            GUUCGCCACCGUCAUGAUUGCCAUAGCGAUGCGCGGGUGAGCUGCUUCGGCGGCUCGCCCGUGCAUCU            UCGCUUCCGGGGAGGGUUCUUCGGAACCUUCUGGGACGUCGUUCGCGGCUCGGUUUAAGGUUCGCCU            UAGACCAUUGGGUGAAGUUU</p>


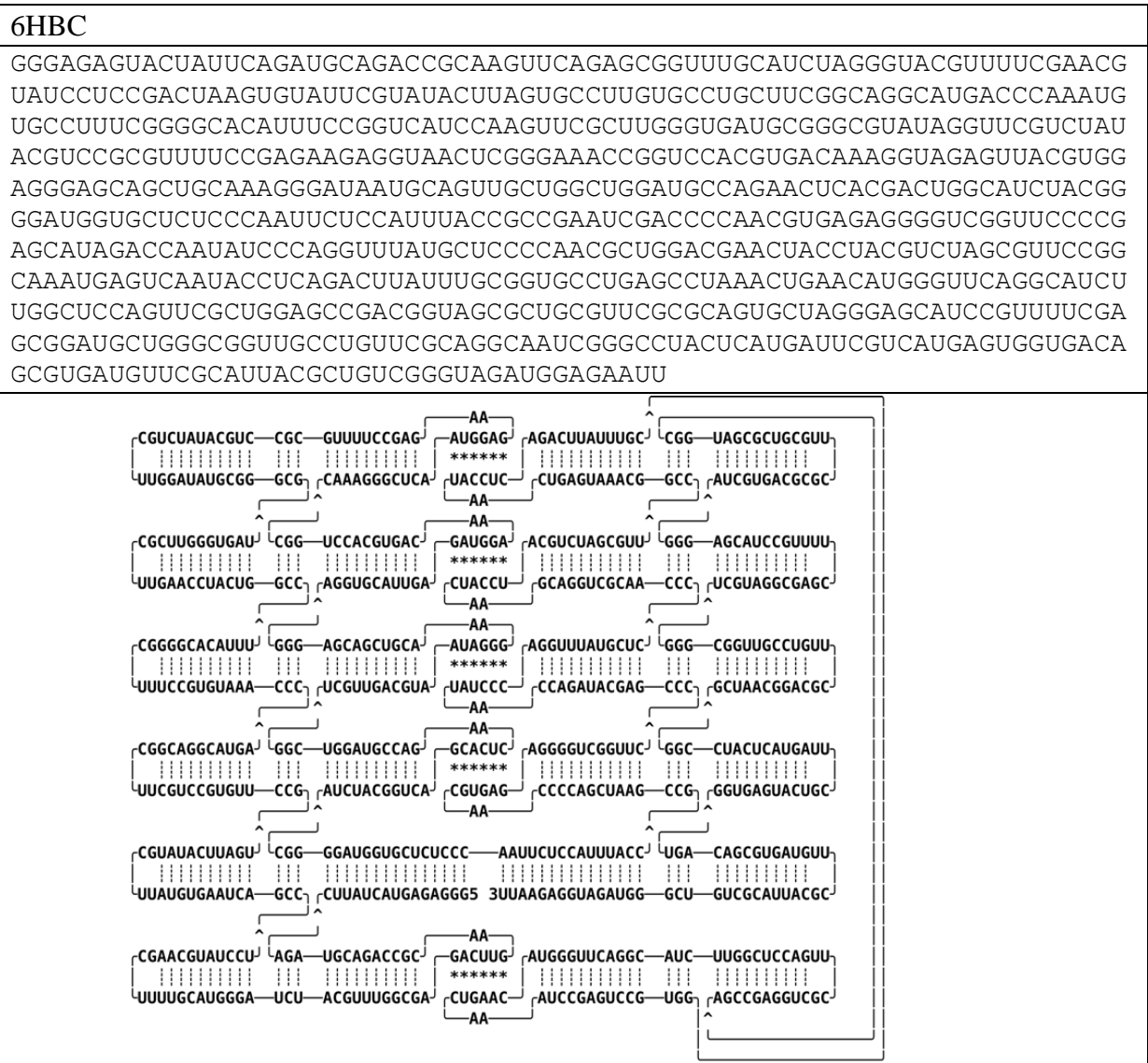
**Supplementary Table 6. RNA sequence and blueprint for 6-helix bundle (6HB).**

6HB

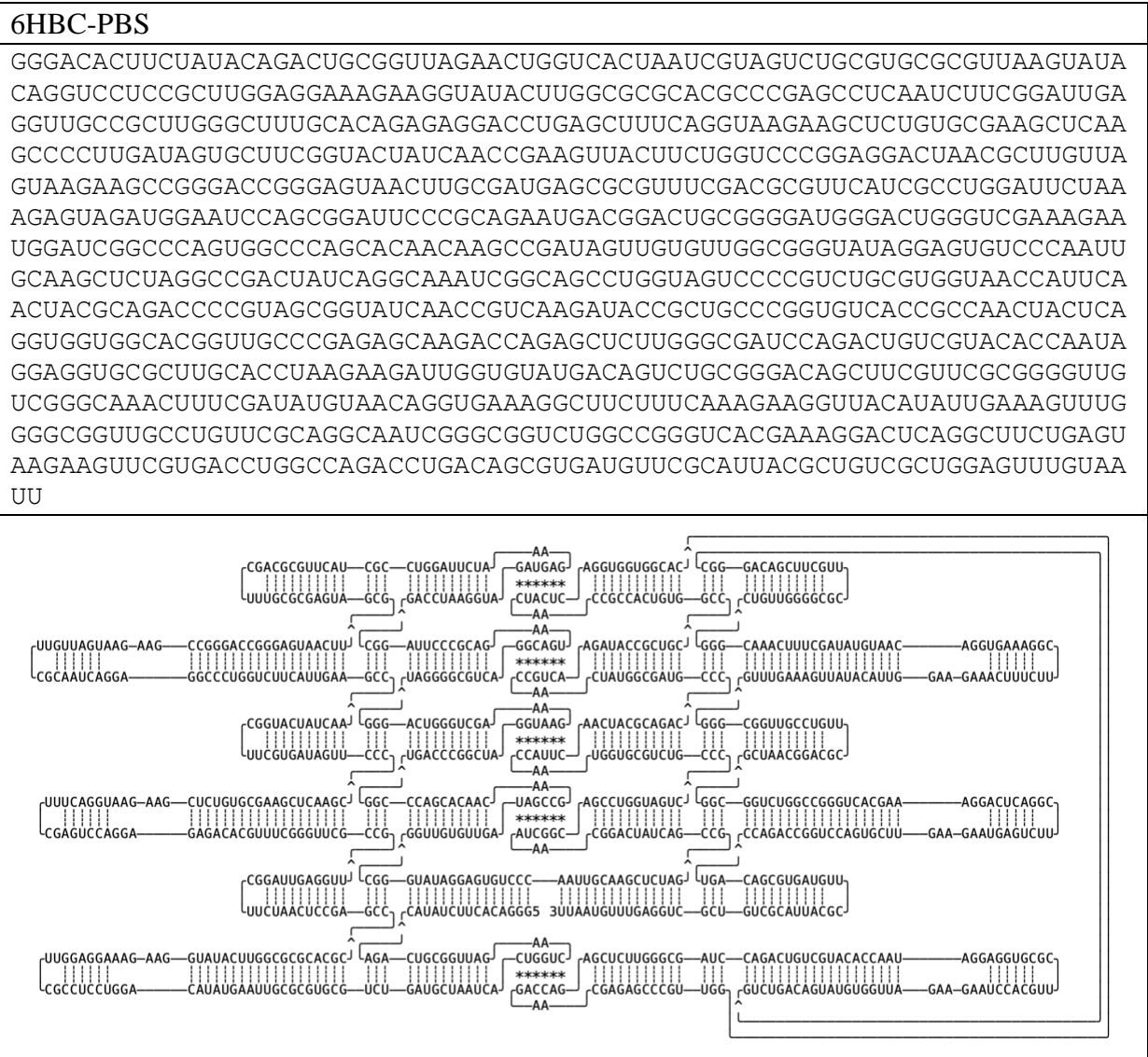
GGGAAAUCCCGCCUGAUACGGUUCACGUUCGCGUGGACCGUCGGGUGGUCCGCUUACGAGCGGGCCA  
 CGGCGACCGUGCAAUGCGUUGCAUGGUCCGGGCUUGCUCGCUACGGCGAGUAAGCGGGGAACUAGAGG  
 UGCGCCUCUGGUUCGGCGCUAUGUGGCUCGCGCUACAUAUGGCCCGGAUUGGGGAACCCCUAACCCCA  
 GUCGGCCCGUUGGGUCACAACGGUUCAGUGAUCCAACCCGGGUAUGGCACAACGCGAUAGUGCUAUAC  
 CGCCGUAUGUUCGGAUGAUGGACCGAGCAUACCCGCACGUGGUGGAACACUCGACCACUACGUGAUU  
 AGGGUGGGGUUCCAGAAUUUGUAUCGUGGCCGACUGAGAACUAACGAGUGAAGUUCUJAGUCCCCG  
 UUUUGAGAUGAACCAUCAACAUCUCGAAACCCGGAUAUCGGUGUAAAUCGCGAACACCGGUAUCGCCG  
 AGCUAACUGUAAGAACCGAACAGUUGGCUCUCAUUAACGGCAAUAGGGGAGCUGUUUJAGACAUGA  
 GCAGCGGCGUUCGCGCCGUGCUGGCGUCCGUUUGAUCCGUCAAAUGGACCGGGCAGUUUAUCUCCGG  
 AUAAGCUGCGGGGUCCGAUGAUUCCGAUCAUUGGACGGCGUCGGGUUGGUGCGCCAACUCGACUGAUC  
 CUUUUACCUACGGGUAGAAGGAUCACAUGAUGCAAGUUCU



**Supplementary Table 7. RNA sequence and blueprint for 6-helix bundle with clasp (6HBC).**



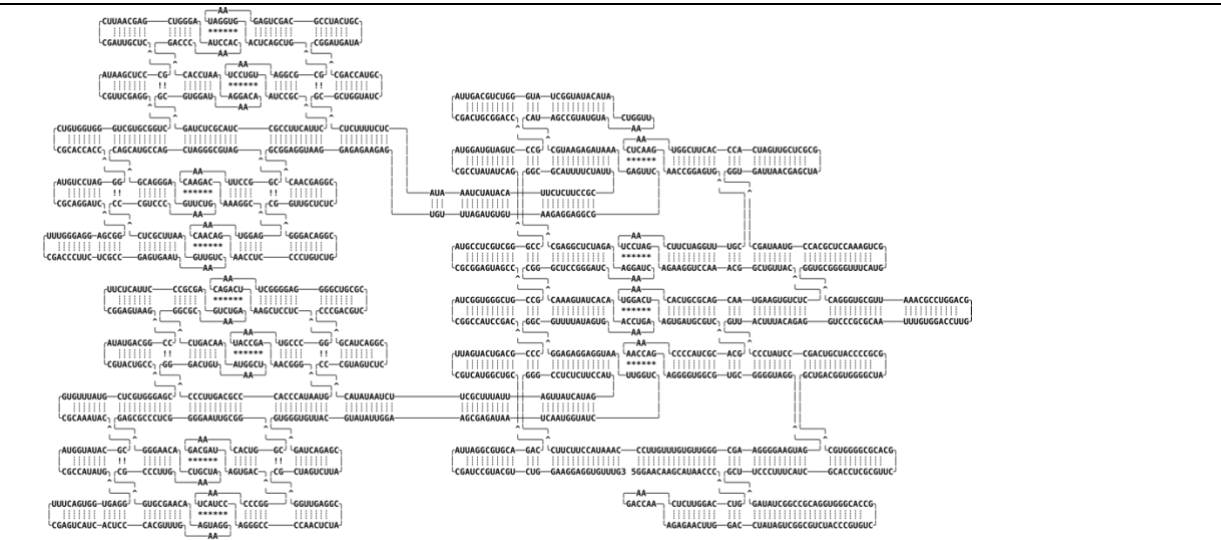
**Supplementary Table 8. RNA sequence and blueprint for 6-helix bundle with clasp and protein binding sites (6HBC-PBS).**



**Supplementary Table 9. RNA sequence and blueprint for 16-helix satellite (6HS).**

**6HS**

GGAACAAGCAUAACCCGUCCAGGUUCUCAAGACCAAAGAGAACUUGGACCUAUAGUCGGCGUCUACCC  
 GUGUCGCCACGGGUGGACGCCGGCUAUAGGCUUCCUUUCAUCGCACCUCGCGUUCGCACGCGGGGUG  
 CGCUGACGGUGGGGCUAGCGCCCAUCGUCAGCCUAUCCGUAUACUUUACAGAGGUCCCGCGCAAUU  
 UGUGGACCUUGGCAGGUCCGCAAUUGCGUGGGACGGUGCGGGGUUCAUGGCUGAAACCUCGCACCG  
 UAAUAGCGGUGAUUAACGAGCUAGCGCUCGUUGAUCACCCACUUCGGUAACUCAAGAACCAGGAGUGCG  
 UUUGGAUCUCAAUCCUAGAGAAGGUCCAAACGGCUGUUAACCUCUGUGAAGUAACGACGCGUCACAAU  
 GGACUAGUGAUGCGUCGCACGCUACCCCAAACAGAGGGGUGGCGUGCGGGGUAGGGGAUGAAGGGGA  
 AGCGGGUUGUGUUUGUUCCAAUACCUUCUUCGGGCCUCUCUCCAUGAUACUAUUGAUUAUUUCGC  
 UUCUAAUAUACCCCGUAGUCUCCGGACUACGCCCGACGUCCGCGUCGGGGAGGGGCUAACAGACUAAG  
 CUCCUCGGCCCGUAAUACCGAAACGGGGUAAUACCCACCCGAGUUCGCGGGACUGUAAUCGGUAAAC  
 AGUCGGCGCAAAGUCUGAGCGCCCUUACUCUUCGGAGUAAGCCGGCAGUAUACGUACUGCCCGAGGGU  
 GCUCGUUUUGUGCGCAAUACCGCAUAUUGGUACGCCAUAUGGGAGUGGUGACUUUCGAGUCAUCACU  
 CCCAGUUUGAAGGAUGAACAAGCGUGCGCCUUGAAAUCGUCACAAGGGGAGCGCCUCGCGGGAAUU  
 GCGGCGGUCACAAGACGAUAGUGACGGCCCAUUAUCCAGGGCCCAACUCUACGGAGUUGGCUCUAG  
 UCUUACGAGACUAGGUGGGUGUACGUUAUUGGAAGCGAGAUAAUCAUUGGUAUCCUGGUUAAUGGA  
 GGAGAGGGGCGUUUUAUAGUGAAAGUCCAACACUAUGAAACCGGGCUCGCGGAUCAACUAGGAAGAU  
 UCGGAGCGGCGCAUUUUCUAUUCGCCUUCUCUACAUAUCUAAUACUCUUUUCUCGCGCUGGUAUCC  
 GUACCAGCCGGAUGAUACGUCAUCCGCAGCUGAGAAUAGGUGACUCAGCUGGCGCGGAAAUCCUGUAU  
 CCGCCUUAUCUCCGCCUACGCUCUAGGCGUGGAUAAACAGGAAAUCCACGACCCAACACCUAAGGGUC  
 GAGCAAUCCGAUUGCUCGCCUCGAAUACGUUCGAGGCUGGCGUGCUGGGUGGUGUCCGCACCACCG  
 GGAUCCUGUACGCAGGAUCGGCGAGGAGGGUUUCGACCCUUCUCGCCGAGUGAAUAACUGUUGAAUUC  
 GCUCCCGUCCCAAGUCUUGAGGGACGCAGCAUGCCAGCUAGGGCGUAGCGGCCUUAACAAGACAAAG  
 GCGAGGUAACAACAGAACCUCUCCUGUCUGCGGACAGGGCGGUUGCUCUCCGGAGCAACGCGGAGGUA  
 AGGAGAGAAGAGUGUUUAGAUUGUGUAAGAGGAGGCGCUUGAGAAAUAGAGAAUGCCAUAAGCCGUAUGU  
 AAAUUGGUCAUACAUUGGCUAUGGGUCUGCAGUUACGACUGCGGACCGCCUGAUGUAGGUACGCCU  
 AUAUCAGCCGGGUCUCUCCGUACGCGGAGUAGCCGCCGUCGGGUGGCUACGGCAUCCGACCCCGCAG  
 UCAUGAUUCGUCAUGGCUGCCAGACGUGCGGAUUACGAUCCGUACGUCUGGAAGGAGGUGUUUG



**Supplementary Table 10. Cryo-EM data collection, refinement and validation statistics.**

	5HT-A EMD-13633 PDB 7PTQ	5HT-A-TC EMD-13926 PDB 7QDU	5HT-B EMD-13636 PDB 7PTS	5HT-B-3X EMD-13592	6HB EMD-13627	6HBC-Y1 EMD-13628 PDB 7PTK	6HBC-PBS EMD-13630 PDB 7PTL	6HBC-Y2 EMD-13626	6HBC-M2 EMD-13625
<b>Data collection and processing</b>									
Magnification	130000	130000	130000	130000	130000	130000	130000	130000	130000
Voltage (kV)	300	300	300	300	300	300	300	300	300
Electron exposure (e <sup>-</sup> /Å <sup>2</sup> )	~60	~60	~60	~60	~60	~60	~60	~60	~60
Defocus range (μm)	-0.7 to -2.2	-0.7 to -2.2	-0.7 to -2.2	-0.7 to -2.2	-0.7 to -2.2	-0.7 to -2.2	-0.7 to -2.2	-0.7 to -2.2	-0.7 to -2.2
Pixel size (Å)	0.647	0.647	0.647	0.647	0.647	0.647	0.647	0.86	0.86
Symmetry imposed	None	None	None	None	None	None	None	None	None
Initial particle images (no.)	1434423	605848	229472	588769	258034	2037822	229472	332956	332956
Final particle images (no.)	471934	166751	54260	173322	92383	375961	54260	55036	55657
Map resolution (Å)									
FSC threshold (0.143)	4.08	5.14	5.71	6.50	6.61	5.18	5.71	7.04	7.43
<b>Refinement</b>									
Initial model used (PDB code)	None	None	None	N/A	N/A	None	None	N/A	N/A
Model resolution (Å)									
FSC threshold (0.143)	3.9	4.8	5.3	N/A	N/A	5	4.7	N/A	N/A
Map sharpening <i>B</i> factor (Å <sup>2</sup> )	303	252	306	N/A	N/A	303	302	N/A	N/A
Model composition									
Non-hydrogen atoms	17434	17693	17906	N/A	N/A	23080	23080	N/A	N/A
Hydrogen atoms	5847	5941	6006	N/A	N/A	7743	7743	N/A	N/A
Nucleotide residues	544	552	558	N/A	N/A	720	720	N/A	N/A
R.m.s. deviations									
Bond lengths (Å)	0.014 (0)	0.014 (2)	0.015 (0)	N/A	N/A	0.014 (0)	0.014 (1)	N/A	N/A
Bond angles (°)	1.954 (184)	2.107 (250)	2.307 (798)	N/A	N/A	2.075 (606)	2.051 (332)	N/A	N/A
Validation									
MolProbity score	1.99	2.38	2.49	N/A	N/A	2.25	2.33	N/A	N/A
Clashscore	1.20	4.58	6.22	N/A	N/A	3.08	3.95	N/A	N/A

**Supplementary Table 11. Seam curvature angles  $\phi$  measured from 3DVA of 5HT-A.**

Each row in the table corresponds to two seams of a given RNA origami structure. The seams (S) are numbered from 5' to 3' and helices (H) are numbered from helix 1, which contain the transcription start site.

Component 1						
Seam	S1			S2		
Theta	H1-H2-H3	H2-H3-H4	H3-H4-H5	H1-H2-H3	H2-H3-H4	H3-H4-H5
1	179	140	141	164	145	175
2	179	139	143	160	146	176
3	180	139	144	157	147	175
4	180	138	145	153	147	176
5	179	137	147	149	146	177
6	179	137	148	146	146	177
7	178	136	149	145	146	177
8	177	136	151	143	146	177
9	177	136	152	141	146	178
10	176	135	154	139	146	178
11	176	135	155	138	146	180
12	176	135	156	136	146	180
13	175	135	157	134	146	179
14	174	135	158	133	146	179
15	175	133	161	132	146	178
16	175	133	162	131	146	177
17	175	132	164	130	146	177
18	175	131	166	129	146	176
19	175	129	168	127	146	175
20	175	130	169	127	145	173
Range	6.19	10.63	28.05	37.02	1.67	6.97

Component 2						
Seam	S1			S2		
Theta	H1-H2-H3	H2-H3-H4	H3-H4-H5	H1-H2-H3	H2-H3-H4	H3-H4-H5
1	150	158	149	143	155	175
2	159	160	147	144	155	175
3	158	160	147	142	156	174
4	157	158	149	142	156	173
5	154	158	151	143	154	173
6	155	159	146	144	153	174
7	155	156	148	143	153	174
8	155	155	149	143	151	174
9	154	154	150	142	151	174
10	153	154	150	142	151	173
11	151	154	150	142	151	173
12	150	154	149	142	148	174
13	151	154	148	142	143	178
14	151	153	148	144	140	175
15	150	151	150	143	140	176
16	147	150	152	144	145	172
17	147	149	153	144	140	180



18	148	148	152	143	140	179
19	148	150	147	143	141	179
20	149	146	152	143	142	175
Range	11.42	13.81	7.43	2.15	16.30	7.85

Component 3						
Seam	S1			S2		
Theta	H1-H2-H3	H2-H3-H4	H3-H4-H5	H1-H2-H3	H2-H3-H4	H3-H4-H5
1	174	144	153	155	149	174
2	170	140	151	145	153	173
3	170	142	146	144	152	174
4	178	149	144	143	152	173
5	180	150	144	150	146	173
6	178	146	146	148	145	172
7	174	141	145	144	146	172
8	175	140	144	145	144	172
9	177	139	145	144	141	170
10	175	138	144	143	141	173
11	176	138	142	141	141	172
12	179	138	141	140	140	172
13	179	137	140	140	137	171
14	179	137	140	139	135	169
15	179	137	139	136	137	171
16	178	135	137	136	137	173
17	175	138	137	137	136	175
18	179	135	137	137	136	176
19	177	134	136	134	136	175
20	177	130	137	133	135	175
Range	9.68	20.38	17.34	22.37	17.71	7.05

**Supplementary Table 12. Crossover angles  $\theta$  measured from 3DVA of 5HT-A.**

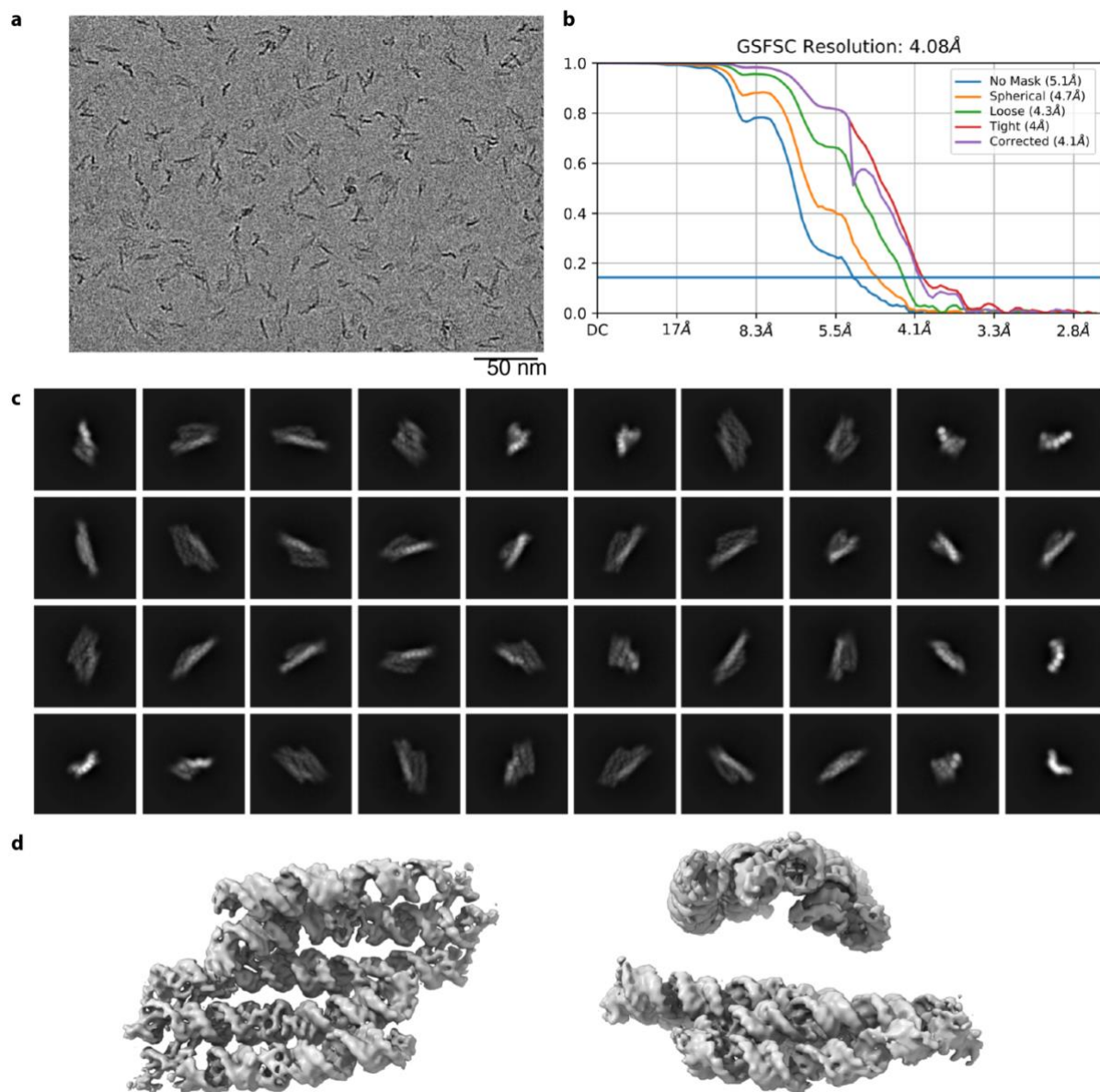
Each row in the table corresponds to two seams of a given RNA origami structure. The seams (S) are numbered from 5' to 3' and helices (H) are numbered from helix 1, which contain the transcription start site.

Component 1								
Seam	S1				S2			
Theta	H1-H2	H2-H3	H3-H4	H4-H5	H1-H2	H2-H3	H3-H4	H4-H5
1	15.2	16.3	25.1	22.3	15.7	20.5	11.4	28.4
2	16.6	16.7	25.0	22.0	16.8	20.6	11.0	28.0
3	18.2	17.0	25.0	21.5	17.6	20.6	10.8	27.5
4	19.4	17.3	25.0	21.1	18.4	20.6	10.7	27.0
5	20.6	17.6	25.1	20.7	19.2	20.6	10.4	26.5
6	22.1	17.8	25.0	20.1	19.9	20.7	10.1	25.9
7	23.3	18.1	24.8	19.6	20.5	20.6	9.8	25.3
8	24.5	18.4	24.7	19.1	21.1	20.7	9.5	24.6
9	25.6	18.6	24.5	18.2	21.7	20.6	9.1	24.0
10	26.9	18.8	24.5	17.7	22.2	20.6	8.9	23.5
11	25.9	19.0	24.4	17.2	22.7	20.6	8.5	22.9
12	26.9	19.4	24.5	16.4	23.3	20.5	8.2	22.2
13	28.0	19.8	24.3	15.7	23.6	20.5	7.9	21.6
14	28.9	20.0	24.3	15.1	24.1	20.6	7.6	20.9
15	29.8	20.2	24.1	14.3	24.4	20.6	7.1	20.2
16	30.6	20.5	24.1	13.6	24.9	20.6	6.8	19.5
17	31.6	20.7	23.9	12.9	25.3	20.7	6.5	18.9
18	32.3	21.0	23.7	12.0	25.7	20.6	6.1	18.2
19	32.9	21.3	23.5	11.2	26.0	20.7	5.7	17.6
20	33.6	21.7	23.5	10.5	26.3	20.5	5.4	16.9
Range	18.5	5.4	1.6	11.9	10.5	0.2	6.0	11.5

Component 2								
Seam	S1				S2			
Theta	H1-H2	H2-H3	H3-H4	H4-H5	H1-H2	H2-H3	H3-H4	H4-H5
1	25.9	20.1	26.4	16.7	21.9	22.2	7.2	24.6
2	26.1	20.0	26.3	17.0	21.9	22.2	7.3	24.6
3	25.8	19.6	26.1	17.0	22.2	22.2	7.5	24.5
4	25.3	19.4	25.7	16.9	22.3	21.9	7.6	24.4
5	25.3	19.2	25.4	17.0	22.4	21.8	7.8	24.3
6	25.2	19.0	24.9	17.0	22.4	21.6	8.0	24.2
7	25.1	18.7	24.7	17.1	22.4	21.5	8.2	24.0
8	25.2	18.4	24.2	17.2	22.6	21.5	8.5	24.0
9	25.1	18.2	24.0	17.2	22.7	21.3	8.8	24.0
10	25.2	18.1	23.7	17.2	22.8	21.4	9.1	23.9
11	25.4	18.0	23.2	17.2	22.9	21.3	9.4	23.7
12	25.9	17.6	23.1	17.5	23.0	21.3	9.9	23.7
13	26.3	17.3	22.7	17.6	23.0	21.2	10.2	23.5
14	26.7	17.0	22.6	17.8	23.1	21.2	10.5	23.5
15	27.5	16.7	22.4	17.9	23.3	21.5	11.3	23.4
16	28.8	16.5	22.1	18.0	23.3	21.7	12.1	23.4
17	30.6	16.4	21.8	17.9	23.4	22.0	13.1	23.5
18	31.9	16.4	21.5	18.2	23.5	22.6	14.4	23.4

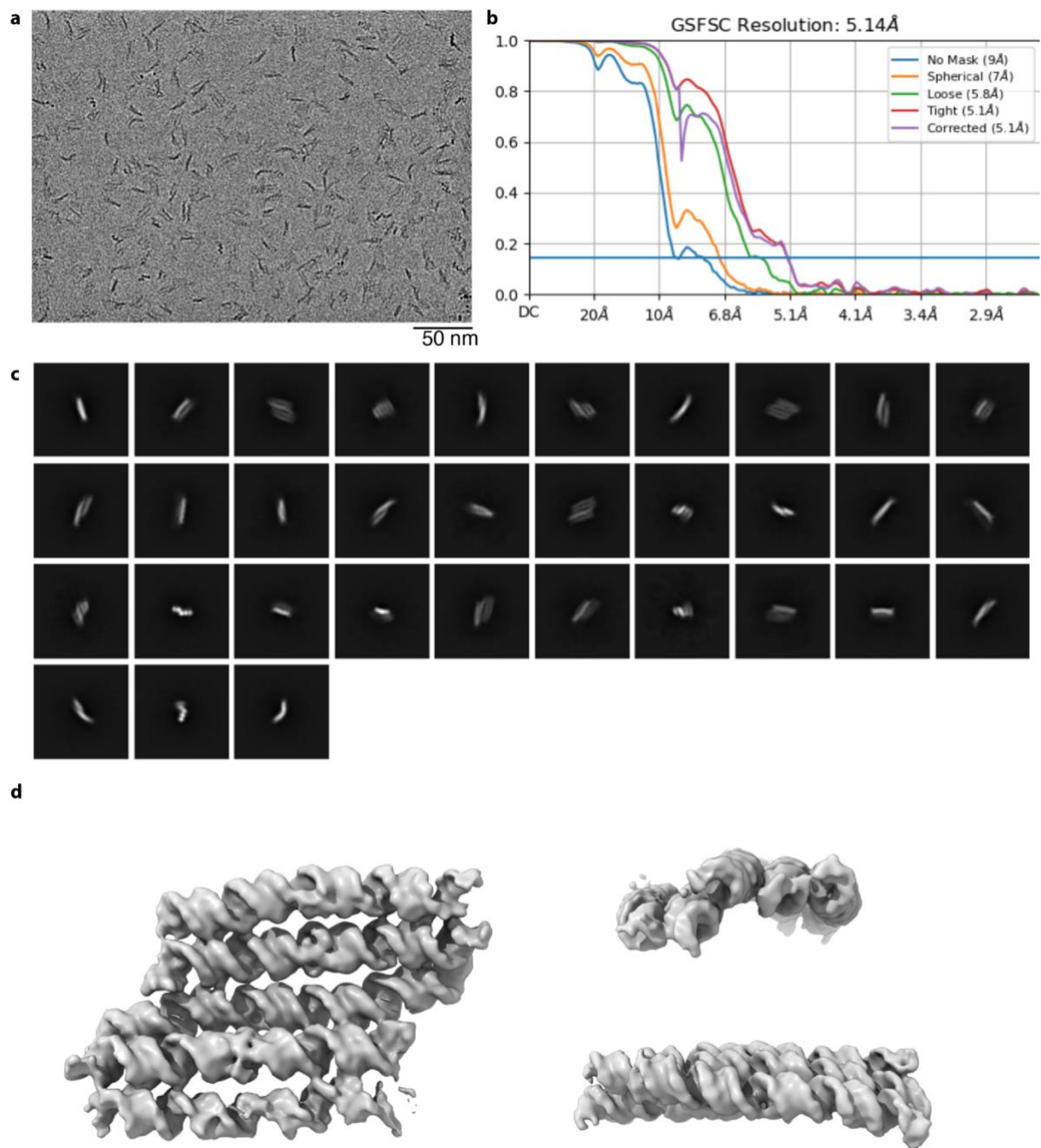
19	33.7	16.1	21.2	18.3	23.5	22.8	14.9	23.4
20	35.7	15.7	21.0	18.2	23.5	23.3	15.8	23.4
Range	10.6	4.4	5.4	1.6	1.6	2.1	8.6	1.3

Component 3								
Seam	S1				S2			
Theta	H1-H2	H2-H3	H3-H4	H4-H5	H1-H2	H2-H3	H3-H4	H4-H5
1	20.0	17.5	24.7	16.8	22.2	20.7	9.3	22.2
2	21.0	17.6	24.6	16.7	22.0	20.6	9.3	22.4
3	22.1	17.6	24.3	16.6	22.0	20.7	9.2	22.6
4	22.6	17.6	24.3	16.7	22.0	20.7	9.1	22.7
5	23.2	17.7	24.2	16.9	22.1	20.8	9.0	22.9
6	24.1	17.7	24.0	17.2	22.1	20.8	9.2	23.1
7	24.9	17.7	23.6	17.2	22.3	21.1	9.2	23.3
8	25.7	17.6	23.4	17.2	22.4	21.0	9.1	23.5
9	26.8	17.6	23.3	17.2	22.6	21.2	9.1	23.7
10	27.6	17.6	23.2	17.3	22.8	21.1	9.0	23.9
11	28.2	17.6	23.0	17.4	22.8	21.3	8.9	24.1
12	28.7	17.7	22.8	17.4	22.9	21.2	8.8	24.3
13	29.5	17.9	22.6	17.6	23.1	21.2	8.7	24.5
14	30.3	17.8	22.4	17.8	23.2	21.4	8.7	24.7
15	30.9	17.9	22.0	17.7	23.4	21.4	8.8	25.0
16	31.5	17.8	21.8	17.8	23.4	21.6	8.8	25.3
17	32.1	17.8	21.8	17.9	23.8	21.6	8.7	25.4
18	32.9	18.0	21.6	18.0	23.9	21.6	8.6	25.5
19	31.1	18.0	21.5	18.2	24.0	21.6	8.7	25.9
20	31.4	17.9	21.3	18.3	24.1	21.7	8.7	26.3
Range	12.9	0.5	3.4	1.7	2.1	1.1	0.7	4.1



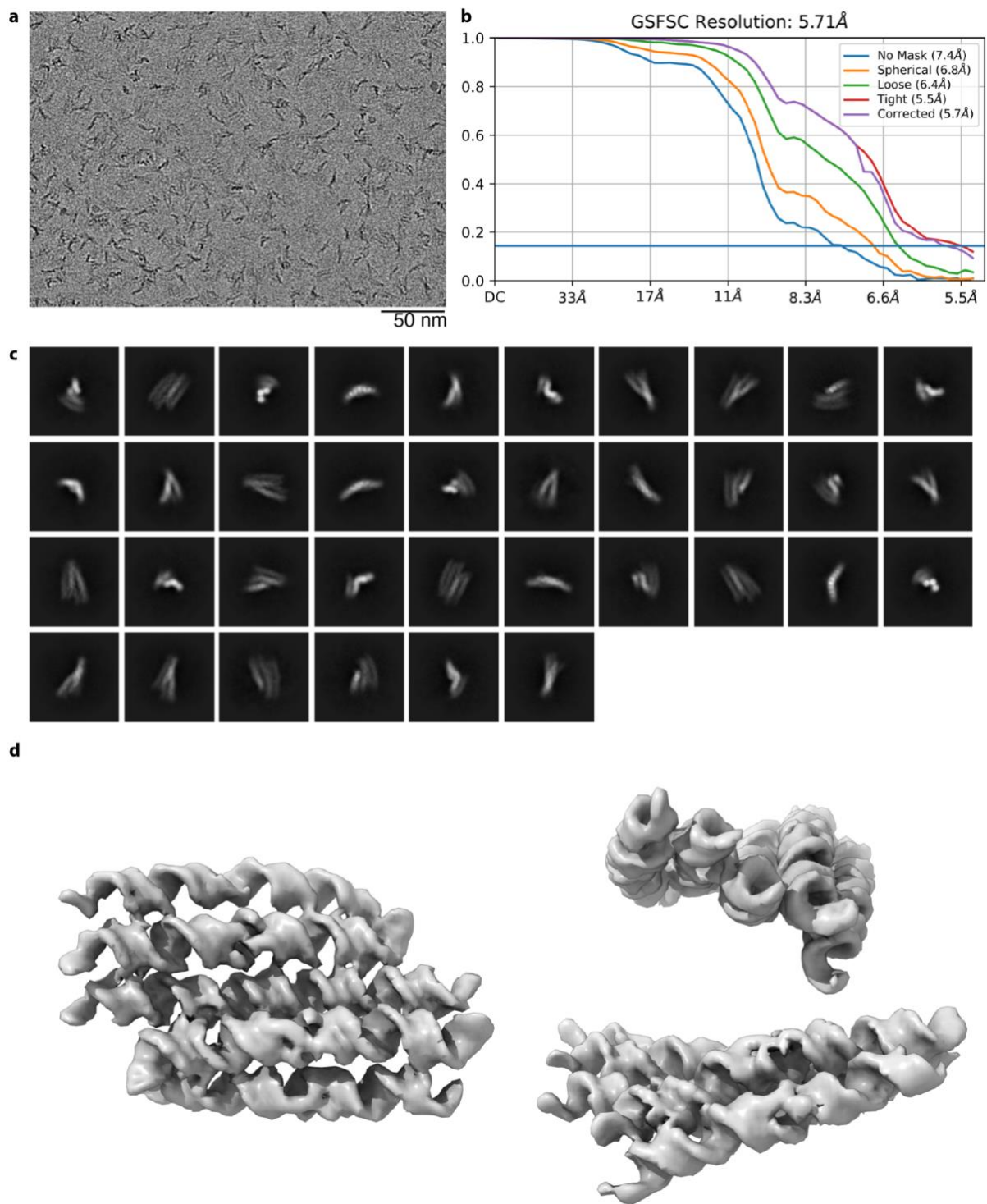
**Supplementary Fig. 1. Cryo-EM data and reconstruction of 5HT-A.**

**a**, Example cryo-EM micrograph from the 5HT-A dataset. **b**, Gold-Standard Fourier Shell Correlation for the 5HT-A reconstruction. **c**, 2D classes from the final particle stack of the 5HT-A dataset. **d**, Three alternate views of the 5HT-A reconstruction.



**Supplementary Fig. 2. Cryo-EM data and reconstruction of 5HT-A-TC.**

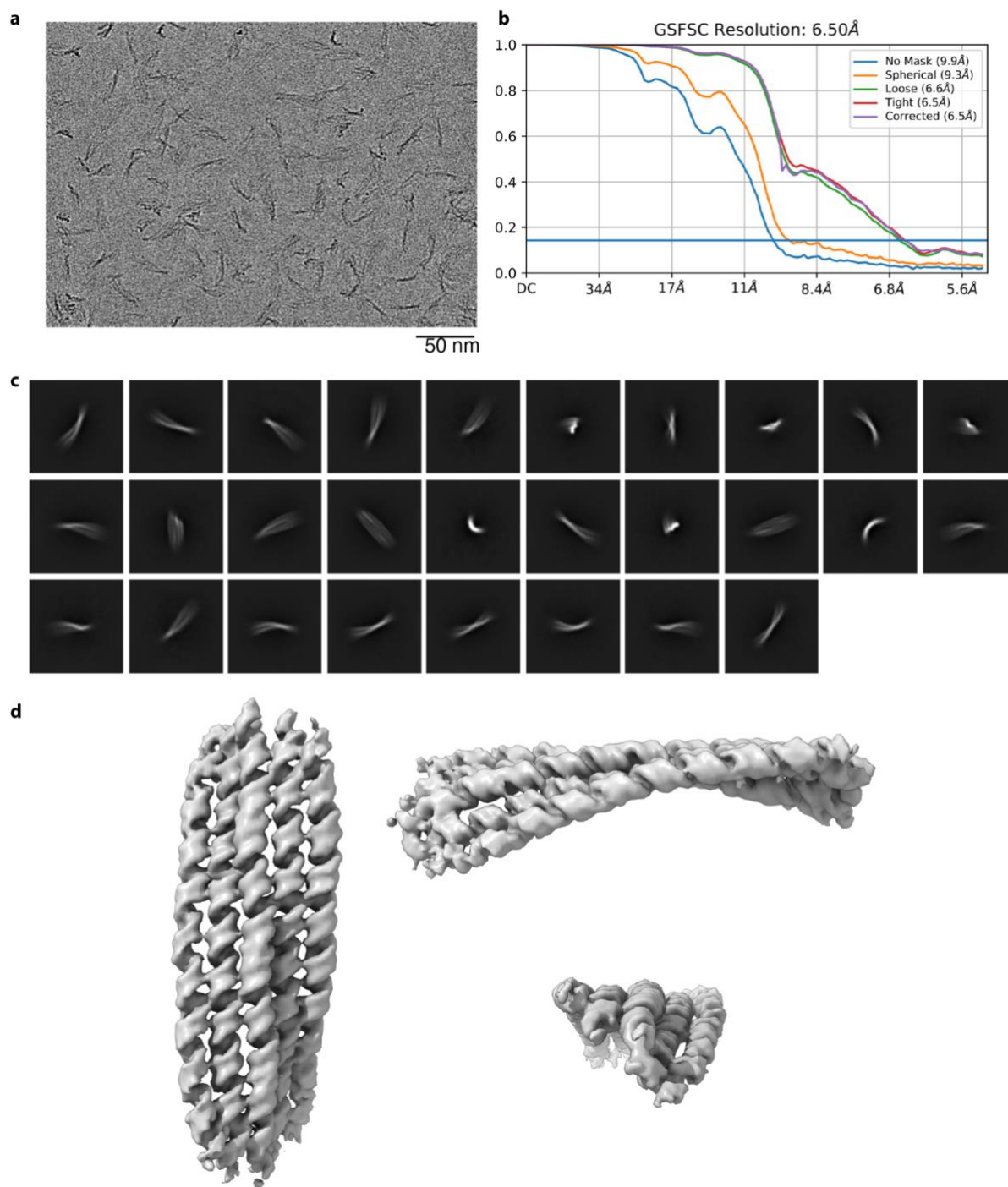
**a**, Example cryo-EM micrograph from the 5HT-A-TC dataset. **b**, Gold-Standard Fourier Shell Correlation for the 5HT-A-TC reconstruction. **c**, 2D classes from the final particle stack of the 5HT-B-3X dataset. **d**, Three alternate views of the 5HT-A-TC reconstruction.



**Supplementary Fig. 3. Cryo-EM data and reconstruction of 5HT-B.**

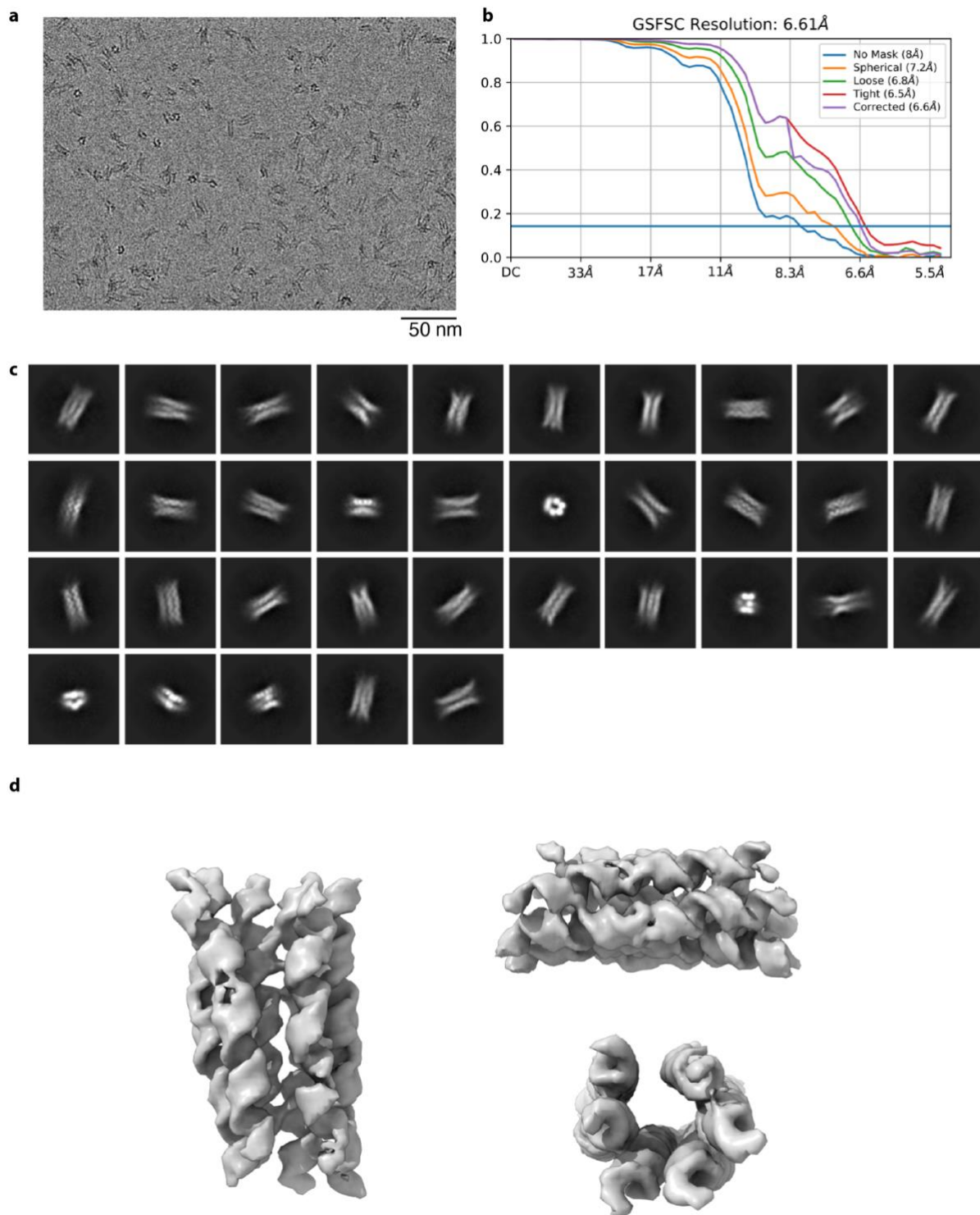
**a**, Example cryo-EM micrograph from the 5HT-B dataset. **b**, Gold-Standard Fourier Shell Correlation for the 5HT-B reconstruction. **c**, 2D classes from the final particle stack of the 5HT-B dataset. **d**, Three alternate views of the 5HT-B reconstruction.





**Supplementary Fig. 4. Cryo-EM data and reconstruction of 5HT-B-3X.**

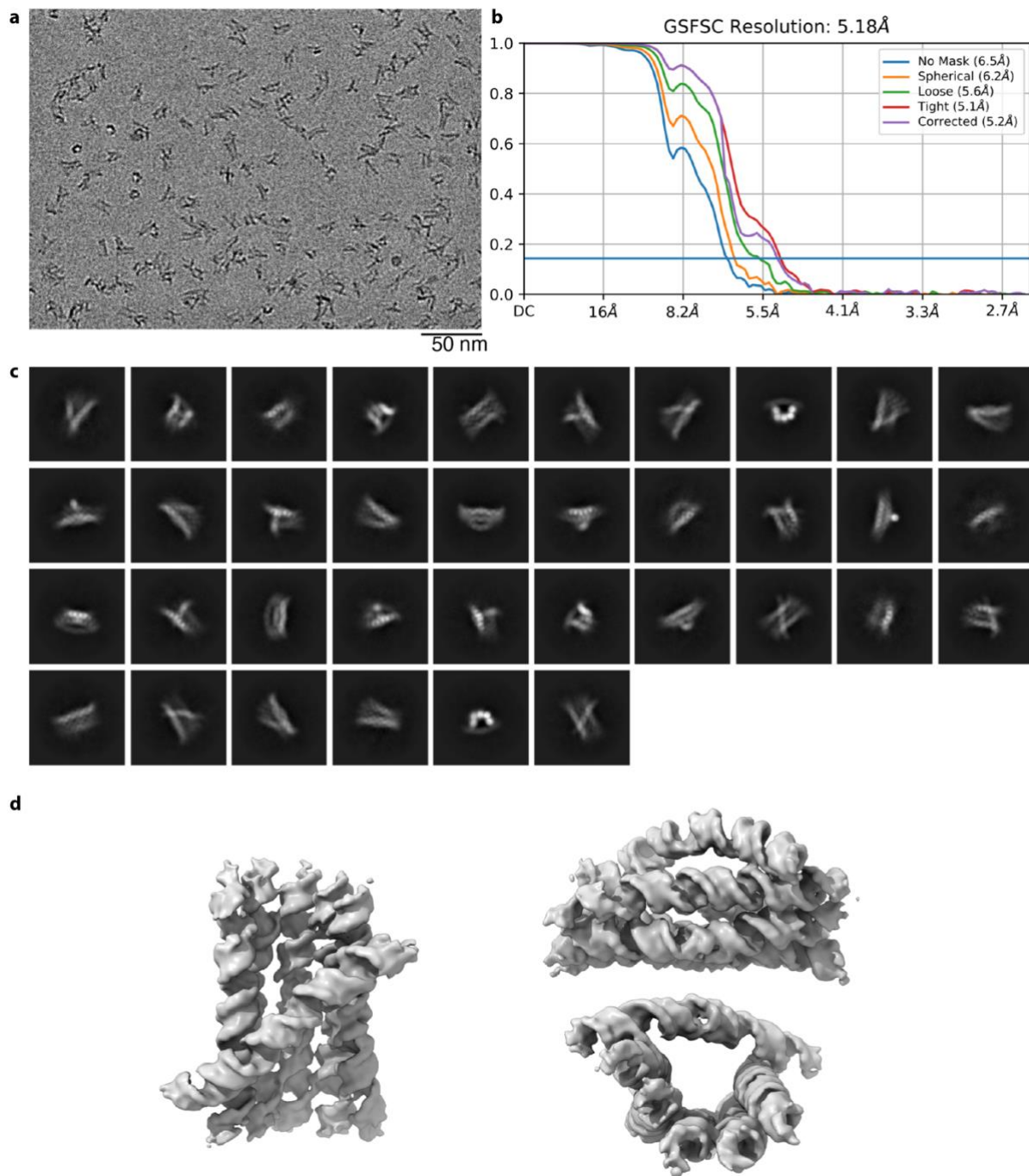
**a**, Example cryo-EM micrograph from the 5HT-B-3X dataset. **b**, Gold-Standard Fourier Shell Correlation for the 5HT-B-3X reconstruction. **c**, 2D classes from the final particle stack of the 5HT-B-3X dataset. **d**, Three alternate views of the 5HT-B-3X reconstruction.



**Supplementary Fig. 5. Cryo-EM data and reconstruction of 6HB.**

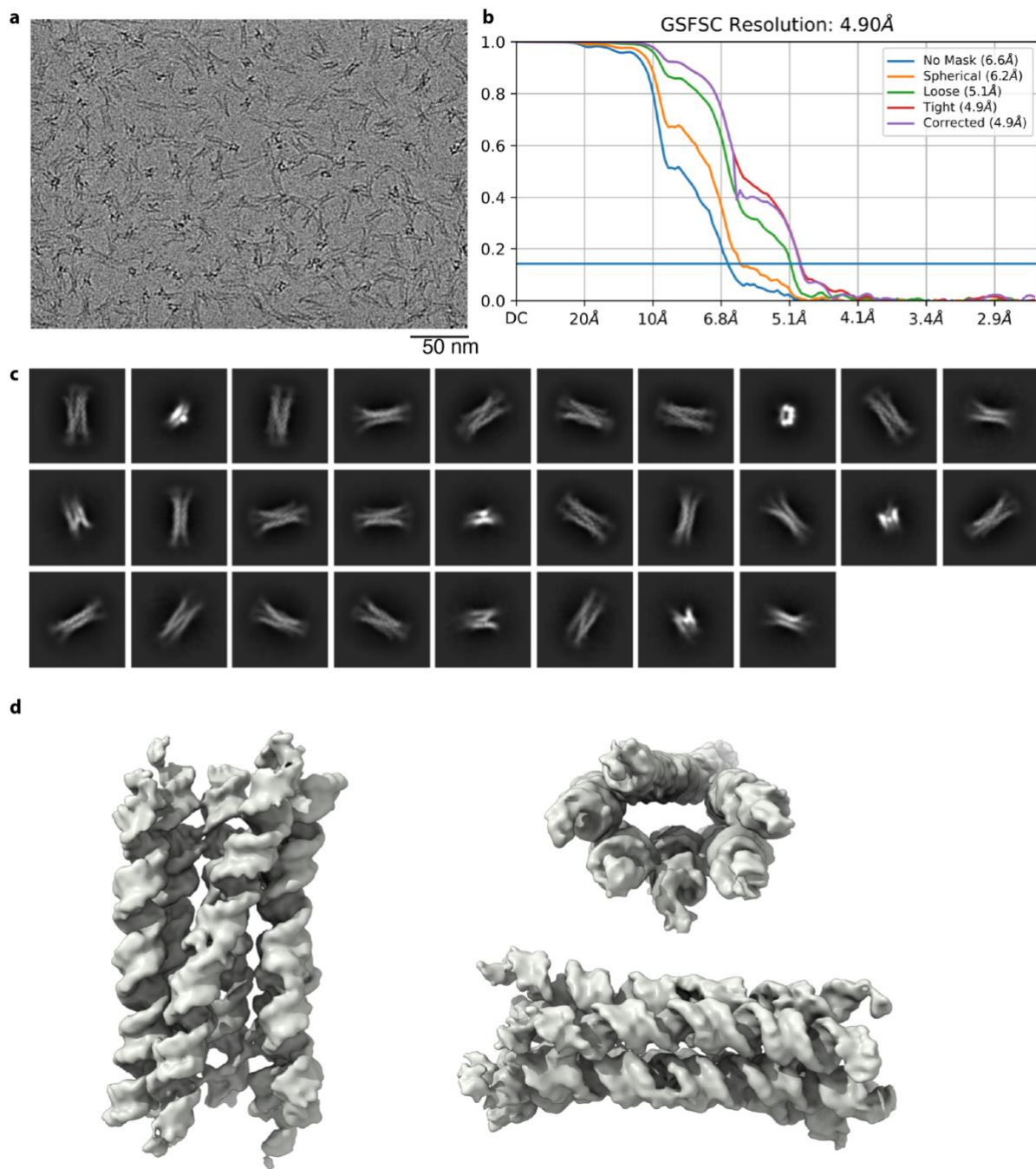
**a**, Example cryo-EM micrograph from the 6HB dataset. **b**, Gold-Standard Fourier Shell Correlation for the 6HB reconstruction. **c**, 2D classes from the final particle stack of the 6HB dataset. **d**, Three alternate views of the 6HB reconstruction.





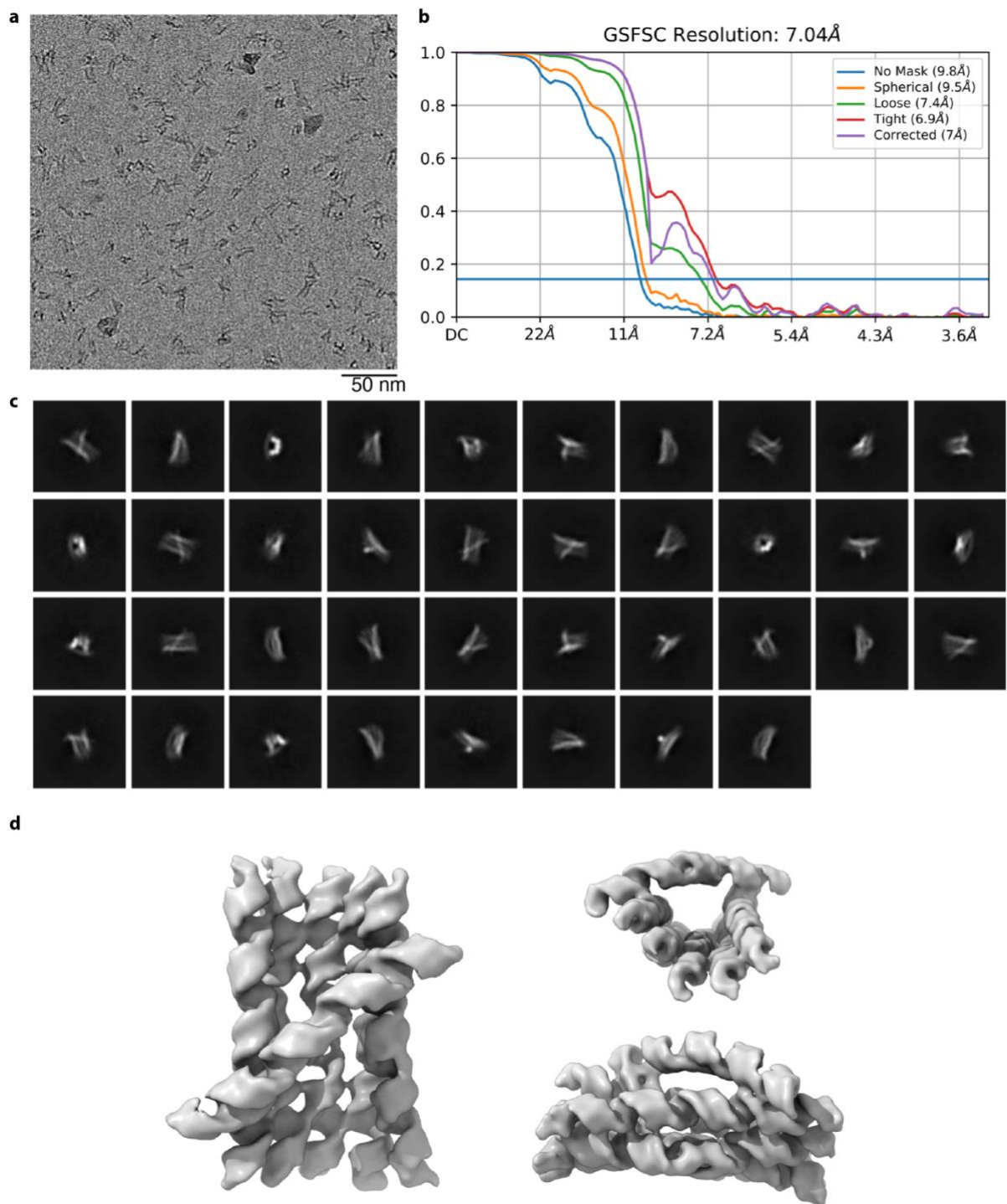
**Supplementary Fig. 6. Cryo-EM data and reconstruction of 6HBC-Young1.**

**a**, Example cryo-EM micrograph from the 6HBC-Young1 dataset. **b**, Gold-Standard Fourier Shell Correlation for the 6HBC-Young1 reconstruction. **c**, 2D classes from the final particle stack of the 6HBC-Young1 dataset. **d**, Three alternate views of the 6HBC-Young1 reconstruction.



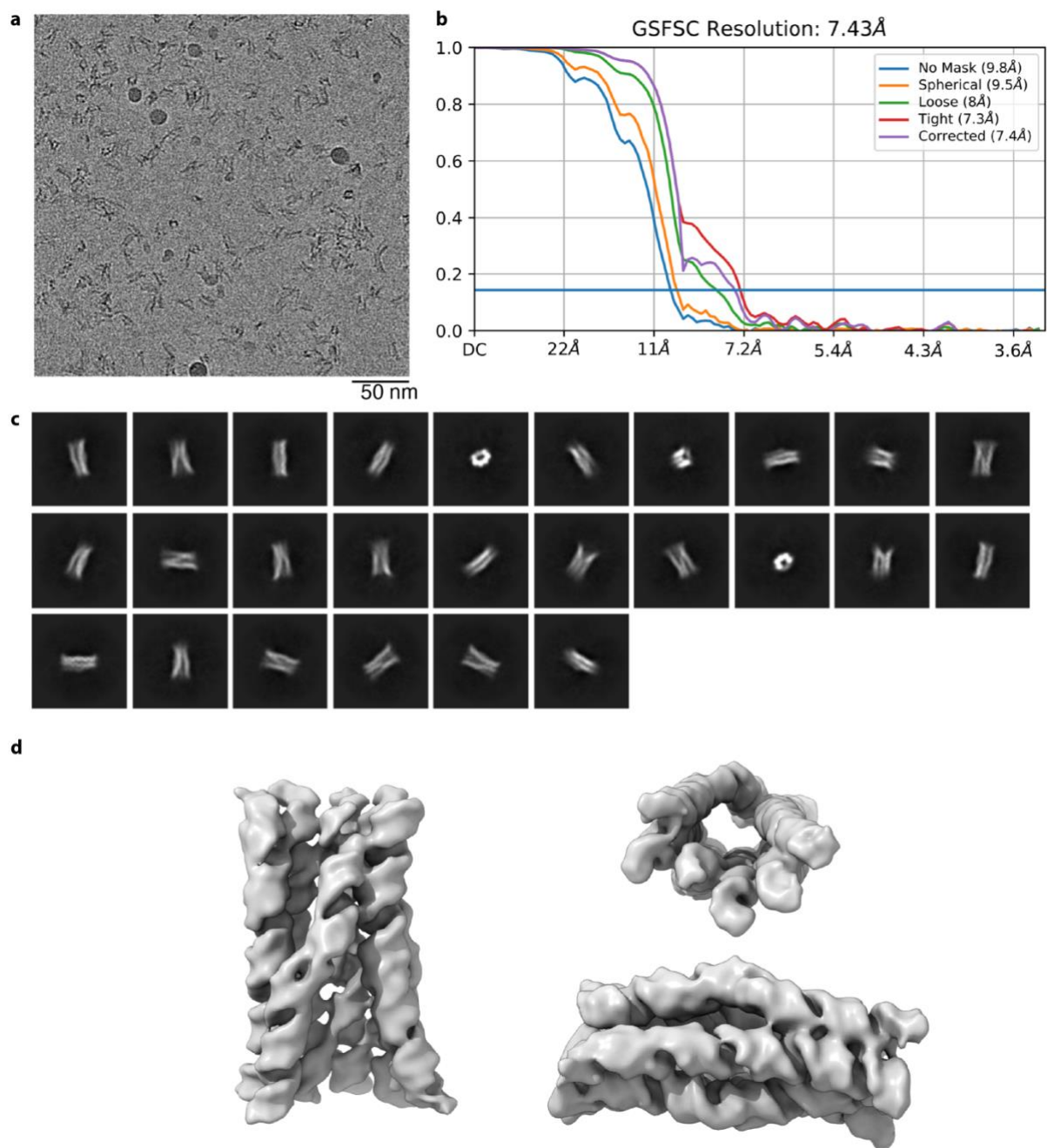
**Supplementary Fig. 7. Cryo-EM data and reconstruction of 6HBC-PBS-Mature1.**

**a**, Example cryo-EM micrograph from the 6HBC-PBS-Mature1 dataset. **b**, Gold-Standard Fourier Shell Correlation for the 6HBC-PBS-Mature1 reconstruction. **c**, 2D classes from the final particle stack of the 6HBC-PBS-Mature1 dataset. **d**, Three alternate views of the 6HBC-PBS-Mature1 reconstruction.



**Supplementary Fig. 8. Cryo-EM data and reconstruction of 6HBC-Young2.**

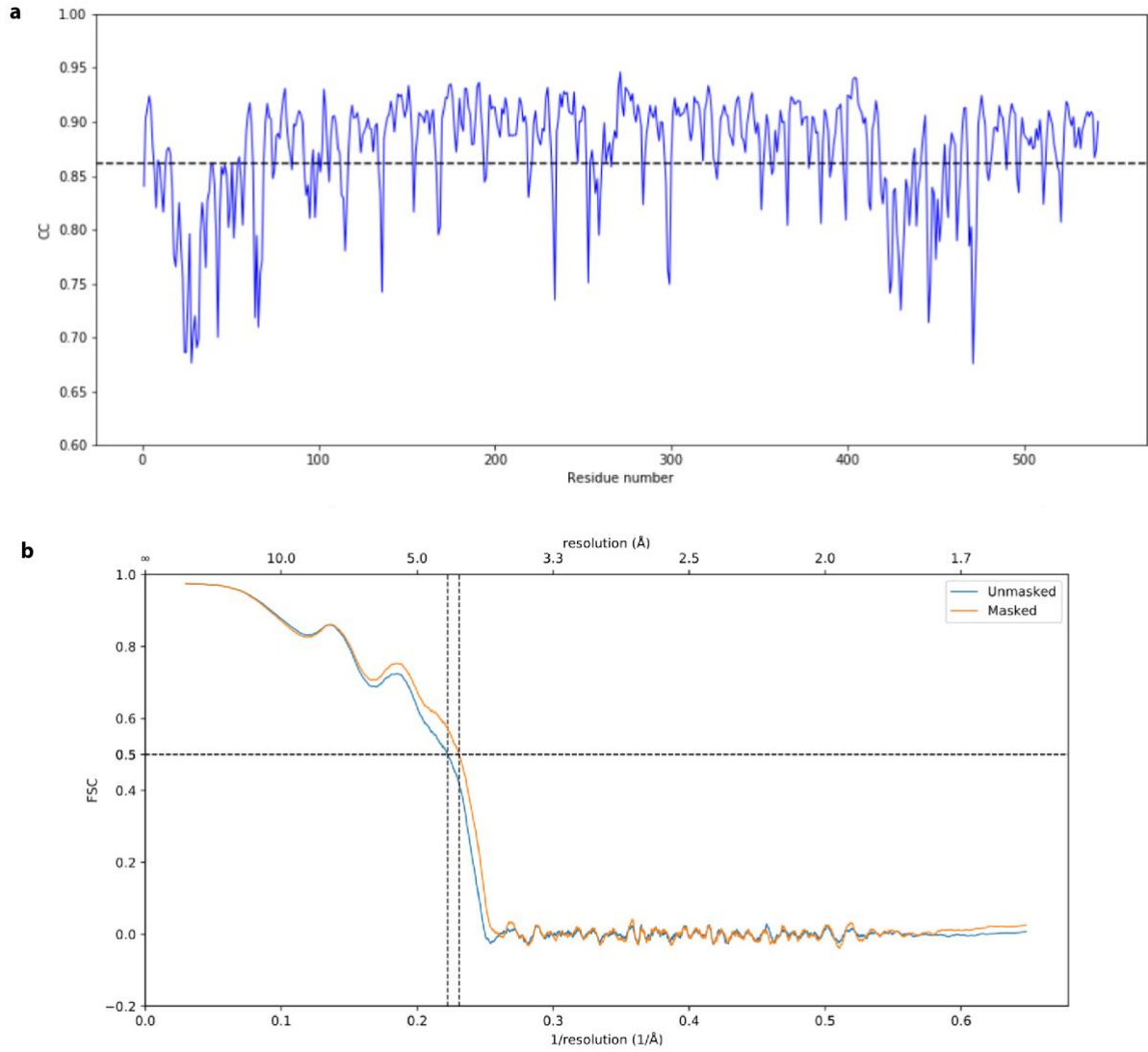
**a**, Example cryo-EM micrograph from the 6HBC-Young2 dataset. **b**, Gold-Standard Fourier Shell Correlation for the 6HBC-Young2 reconstruction. **c**, 2D classes from the final particle stack of the 6HBC-Young2 dataset. **d**, Three alternate views of the 6HBC-Young2 reconstruction.



**Supplementary Fig. 9. Cryo-EM data and reconstruction of 6HBC-Mature2.**

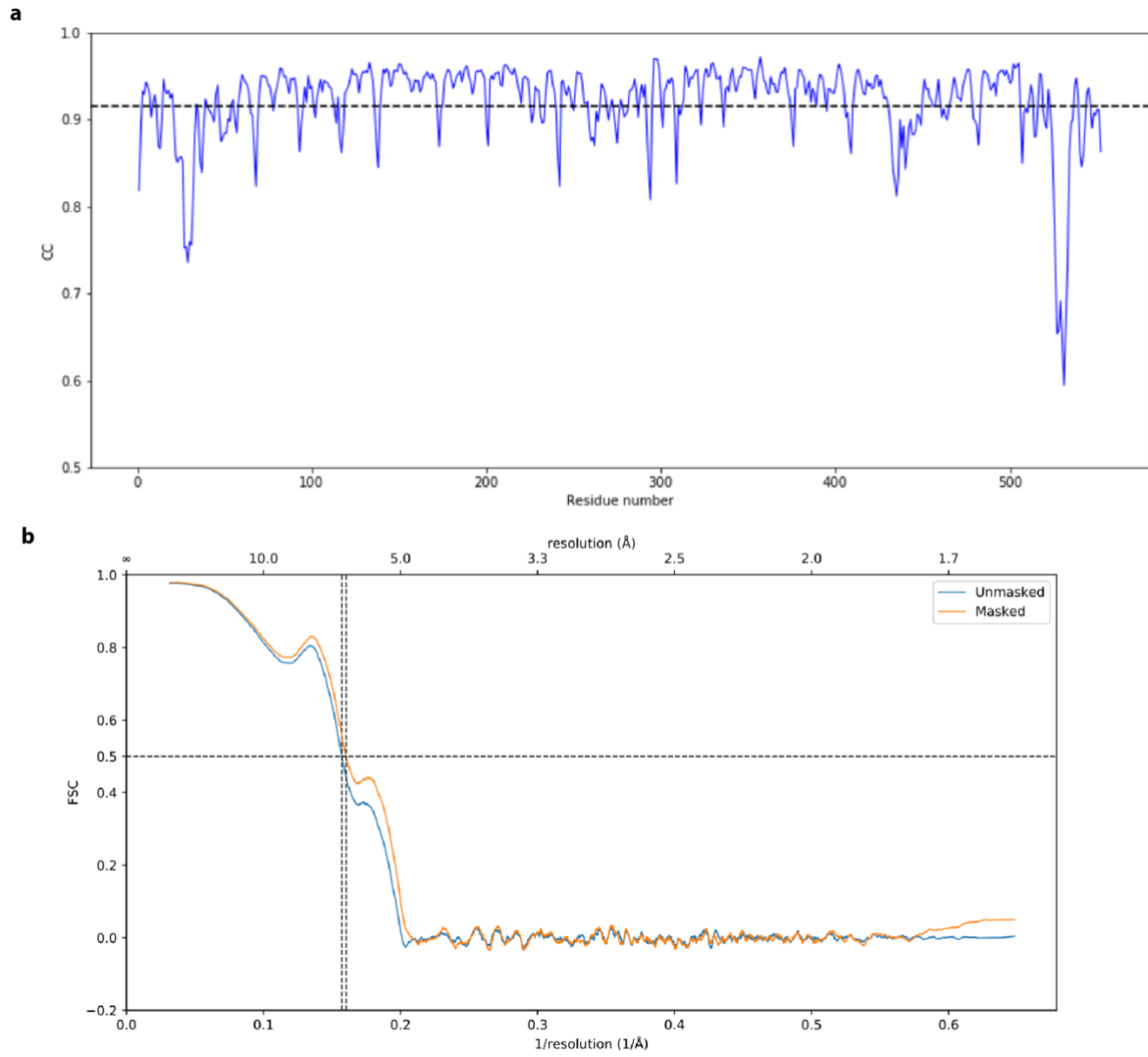
**a**, Example cryo-EM micrograph from the 6HBC-Mature2 dataset. **b**, Gold-Standard Fourier Shell Correlation for the 6HBC-Mature2 reconstruction. **c**, 2D classes from the final particle stack of the 6HBC-Mature2 dataset. **d**, Three alternate views of the 6HBC-Mature2 reconstruction.





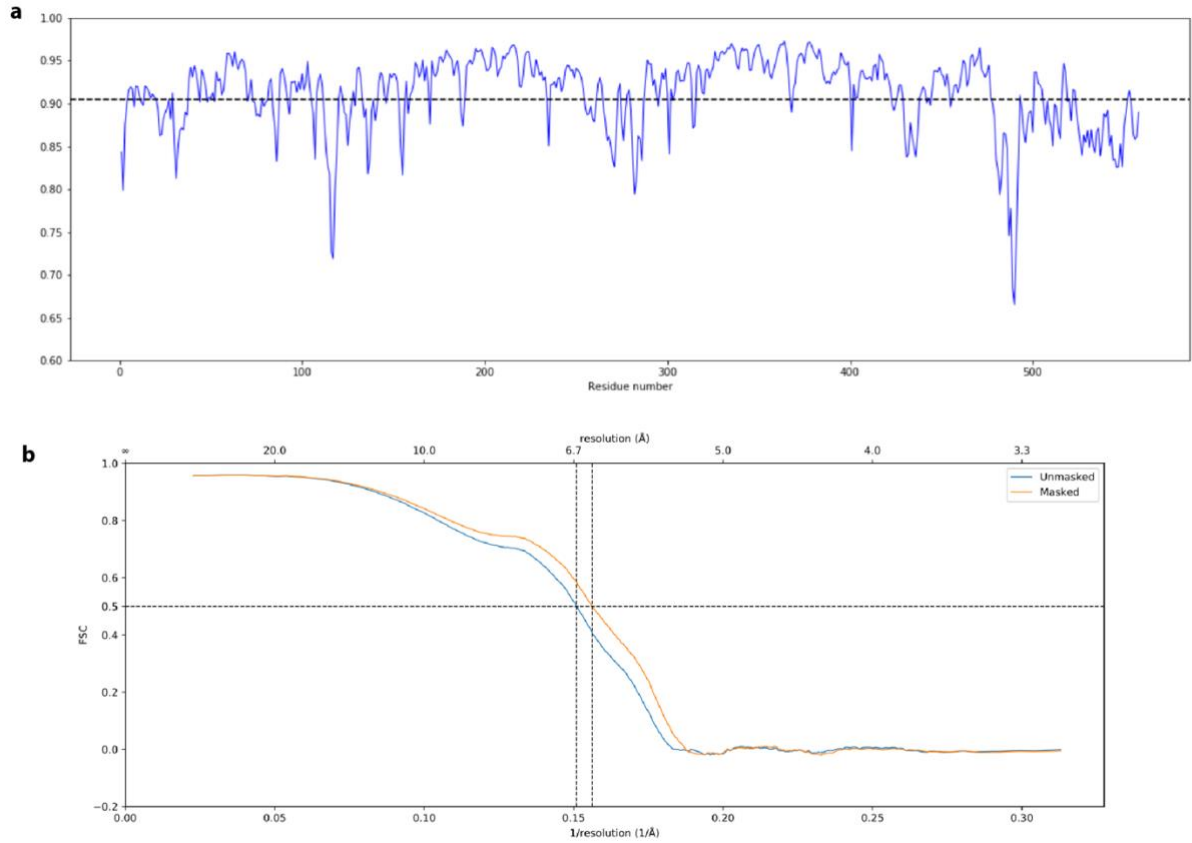
**Supplementary Fig. 10. Map to model correlation of 5HT-A.**

**a**, Per residue cross correlation (CC) and **b**, Fourier shell correlation (FSC) between atomic model and cryo-EM map for 5HT-A.



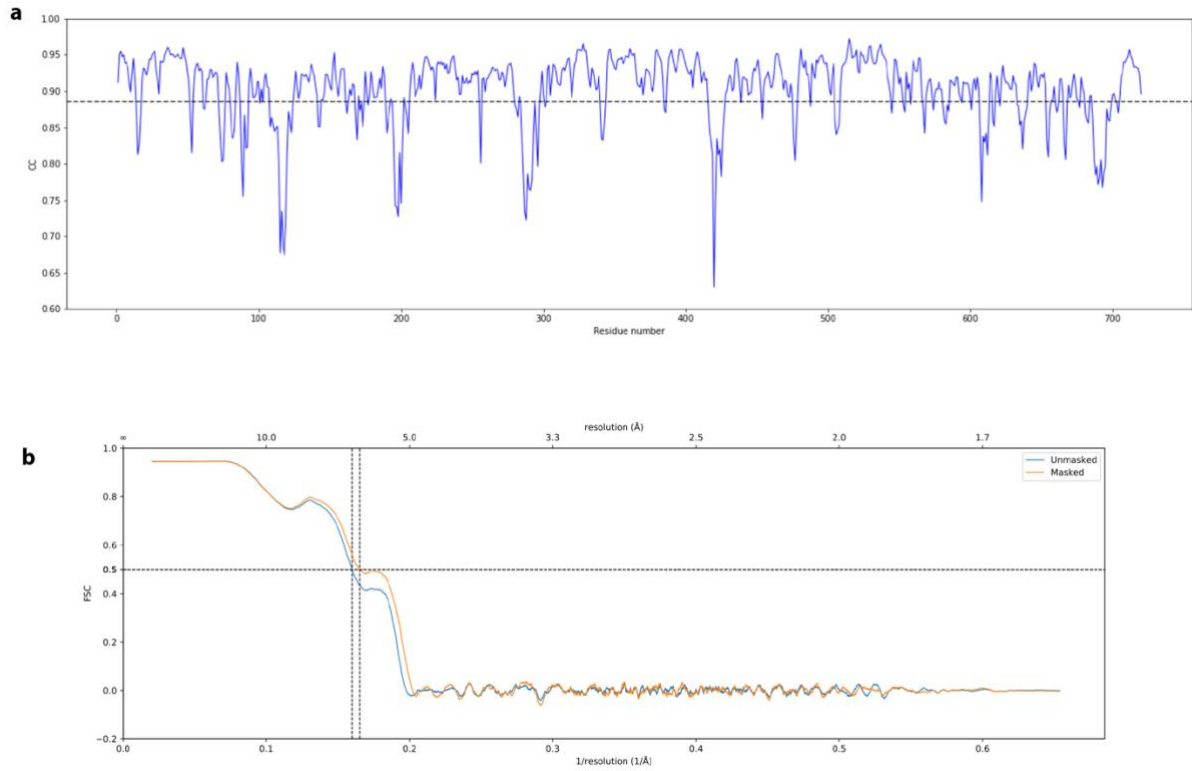
**Supplementary Fig. 11. Map to model correlation of 5HT-A-TC.**

**a**, Per residue cross correlation (CC) and **b**, Fourier shell correlation (FSC) between atomic model and cryo-EM map for 5HT-A-TC.



**Supplementary Fig. 12. Map to model correlation of 5HT-B.**

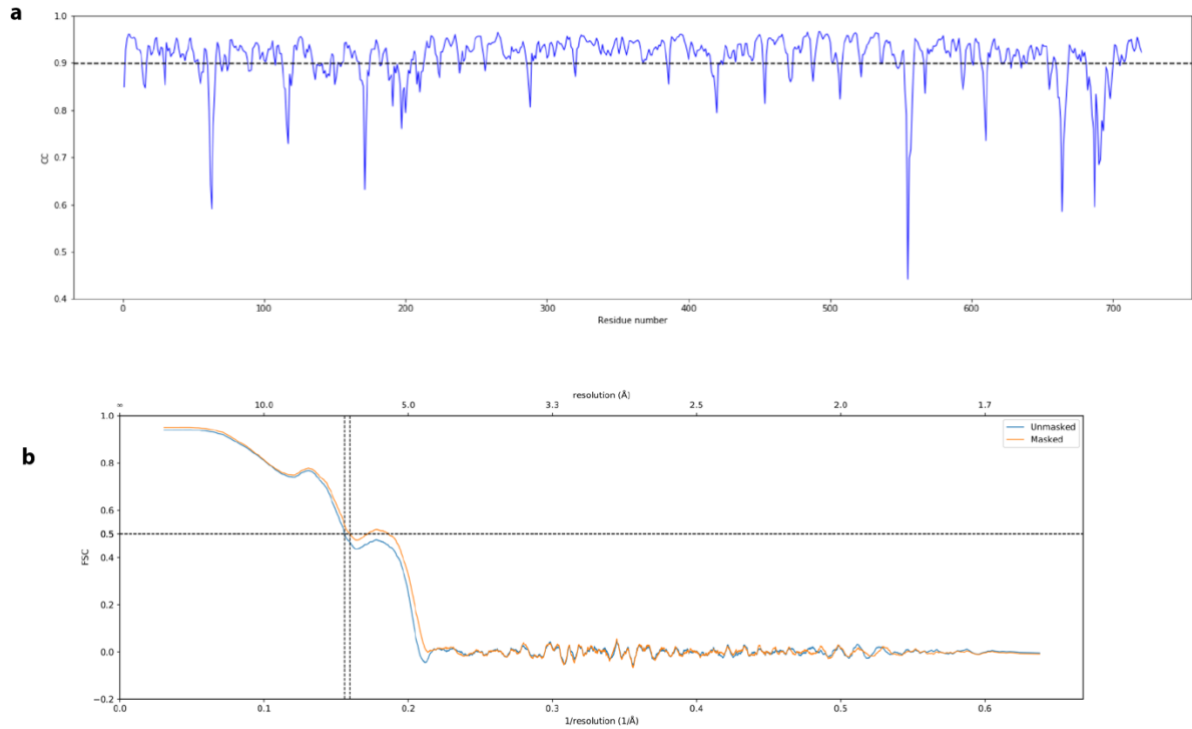
**a**, Per residue cross correlation (CC) and **b**, Fourier shell correlation (FSC) between atomic model and cryo-EM map for 5HT-B.



**Supplementary Fig. 13. Map to model correlation of 6HBC-Young1.**

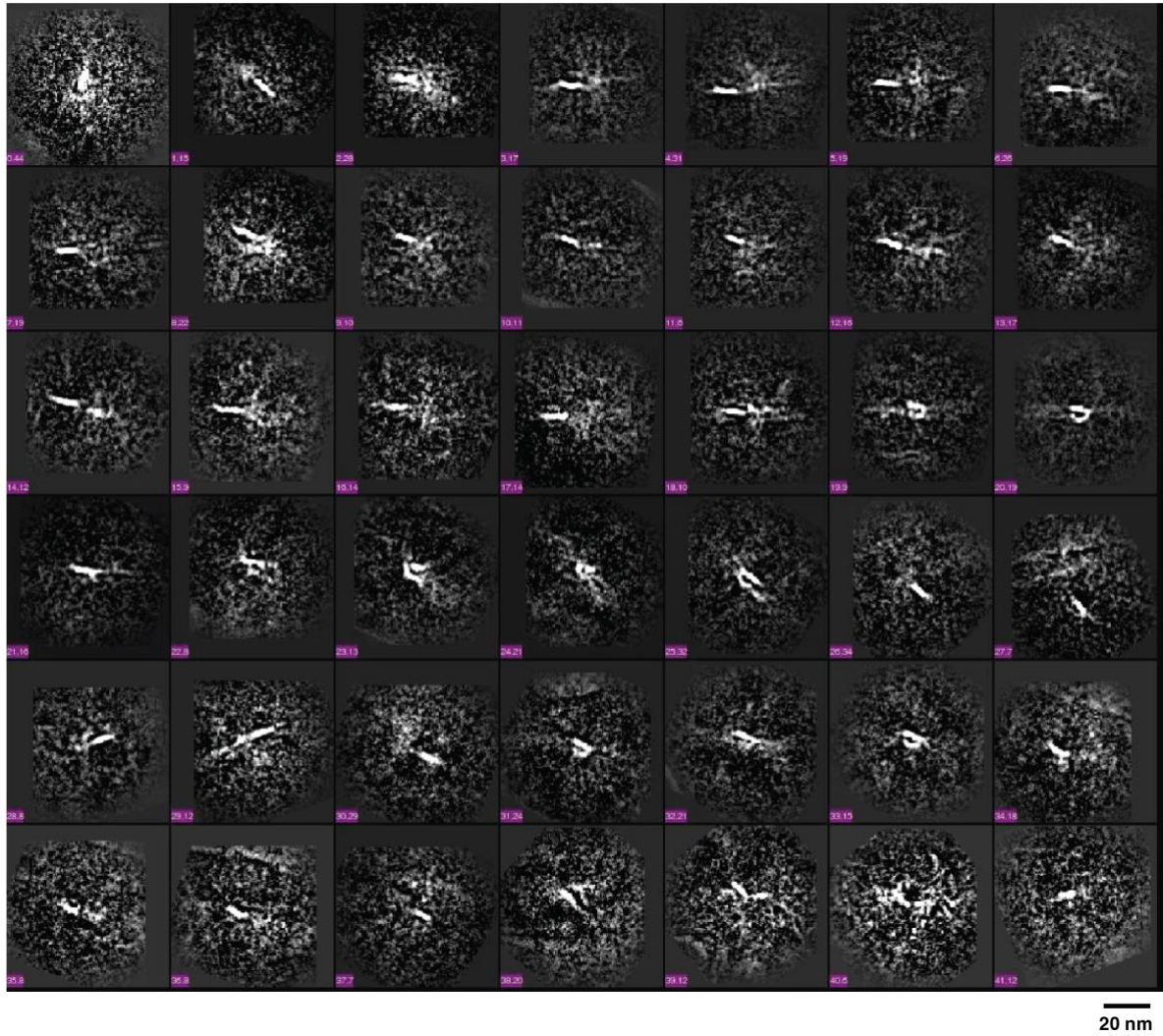
**a**, Per residue cross correlation (CC) and **b**, Fourier shell correlation (FSC) between atomic model and cryo-EM map for 6HBC-Young1.





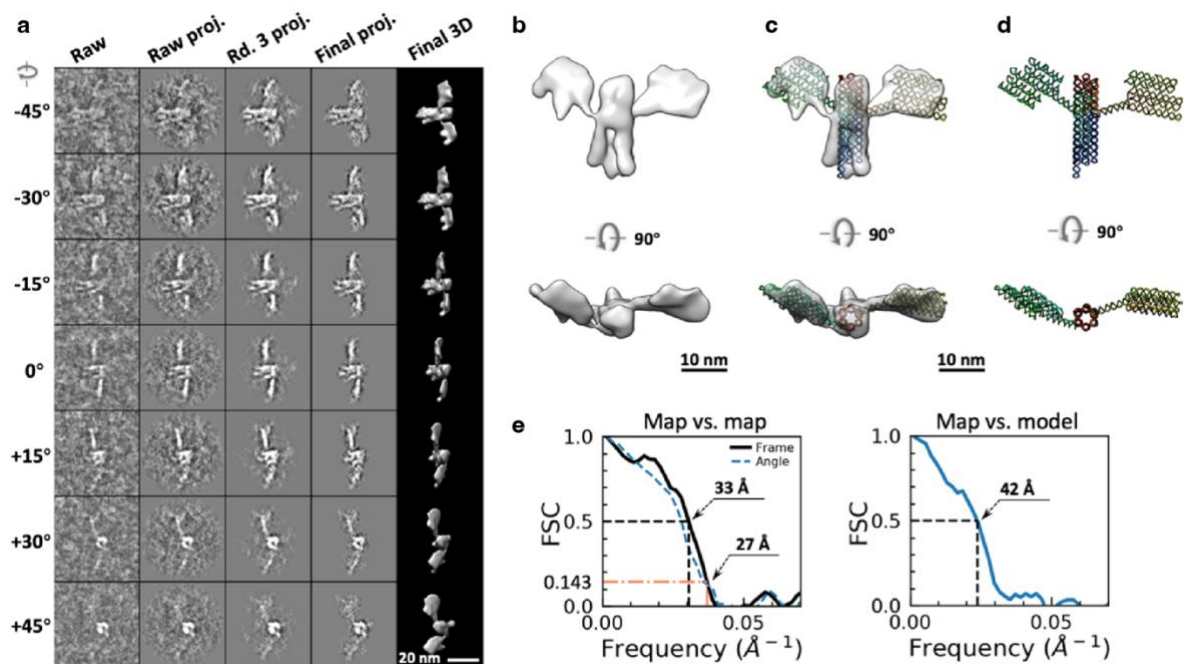
**Supplementary Fig. 14. Map to model correlation of 6HBC-PBS-Mature1.**

**a**, Per residue cross correlation (CC) and **b**, Fourier shell correlation (FSC) between atomic model and cryo-EM map for 6HBC-PBS-Mature1.



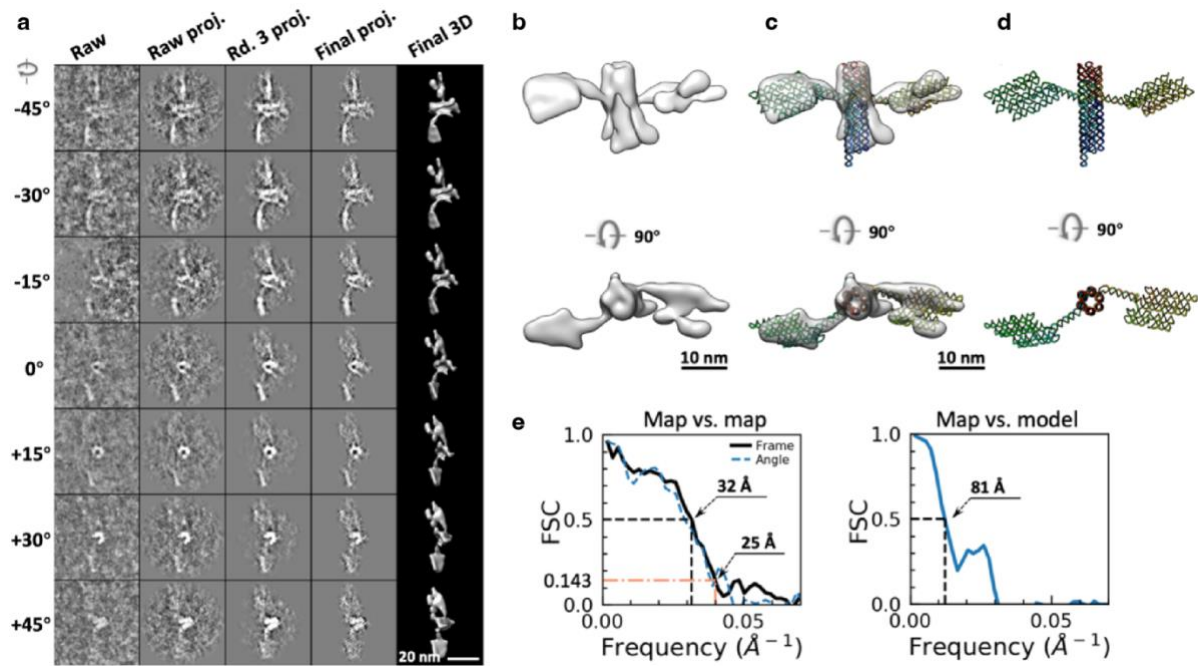
**Supplementary Fig. 15. Cryo-EM 2D class averages of the 16H-satellite sample.**

The reference-free 2D class averages are only able to capture subdomains of the 16H-satellite structure indicating that the sample is not useful for 3D reconstruction. The two numbers on purple rectangle are the index of the class (the first number), and the number of the images used for this class averages (the second number), respectively.



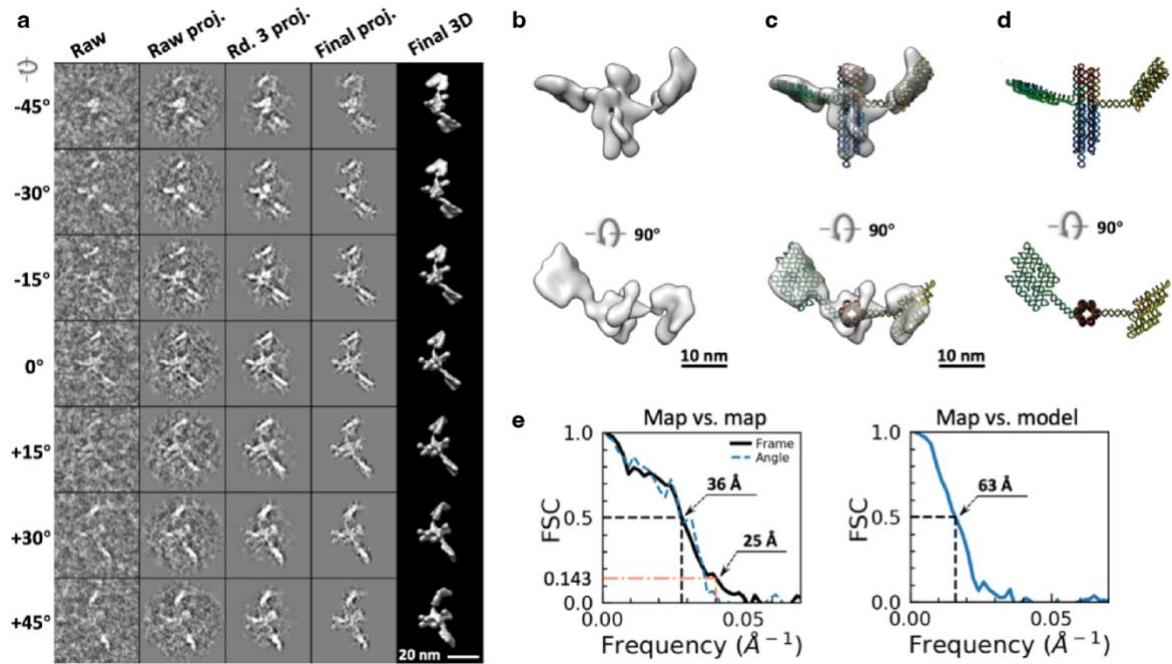
**Supplementary Fig. 16. IPET 3D reconstruction of individual particle #1 of 16HS.**

**a**, Seven representative tilt images of a 16HS particle displayed in the first column from the left. Using IPET, the tilt images are aligned to a common center *via* iterative refinements. The projections of raw, intermediate and final 3D reconstructions at the corresponding tilt angles are displayed in the next four columns. **b**, Two perpendicular views of the final 3D density map; **c**, the map superimposed with the flexible docked model; and **d** the fitted model. **e**, FSC analyses of the final map resolution by two methods, the “map vs. map” (the map reconstructed from the half tilt series, such as even index, against that from the other half tilt series) and “map vs. model” (the map against the density map generated from the model). Two resolutions were measured for “map vs. map” at FSC=0.5 and FSC=0.143 and one resolution was measured for “map vs. model” at FSC=0.5.



**Supplementary Fig. 17. IPET 3D reconstruction of individual particle #2 of 16HS.**

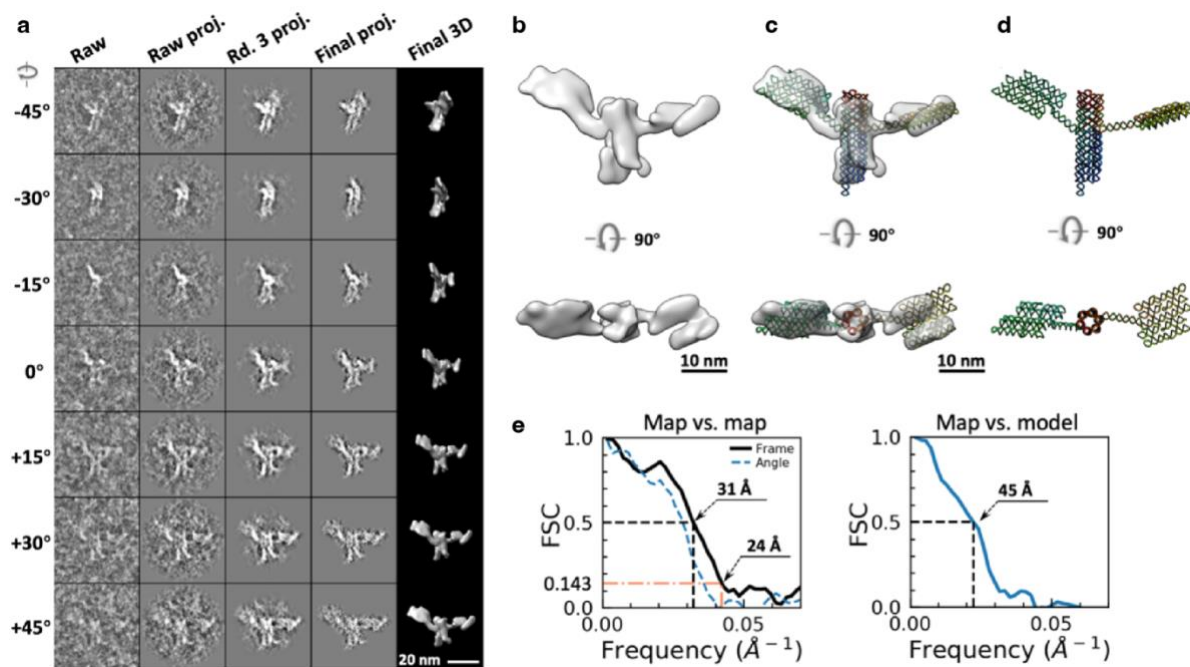
**a**, Seven representative tilt images of a 16HS particle displayed in the first column from the left. Using IPET, the tilt images are aligned to a common center *via* iterative refinements. The projections of raw, intermediate and final 3D reconstructions at the corresponding tilt angles are displayed in the next four columns. **b**, Two perpendicular views of the final 3D density map; **c**, the map superimposed with the flexible docked model; and **d** the fitted model. **e**, FSC analyses of the final map resolution by two methods, the “map vs. map” (the map reconstructed from the half tilt series, such as even index, against that from the other half tilt series) and “map vs. model” (the map against the density map generated from the model). Two resolutions were measured for “map vs. map” at FSC=0.5 and FSC=0.143 and one resolution was measured for “map vs. model” at FSC=0.5.



**Supplementary Fig. 18. IPET 3D reconstruction of individual particle #3 of 16HS.**

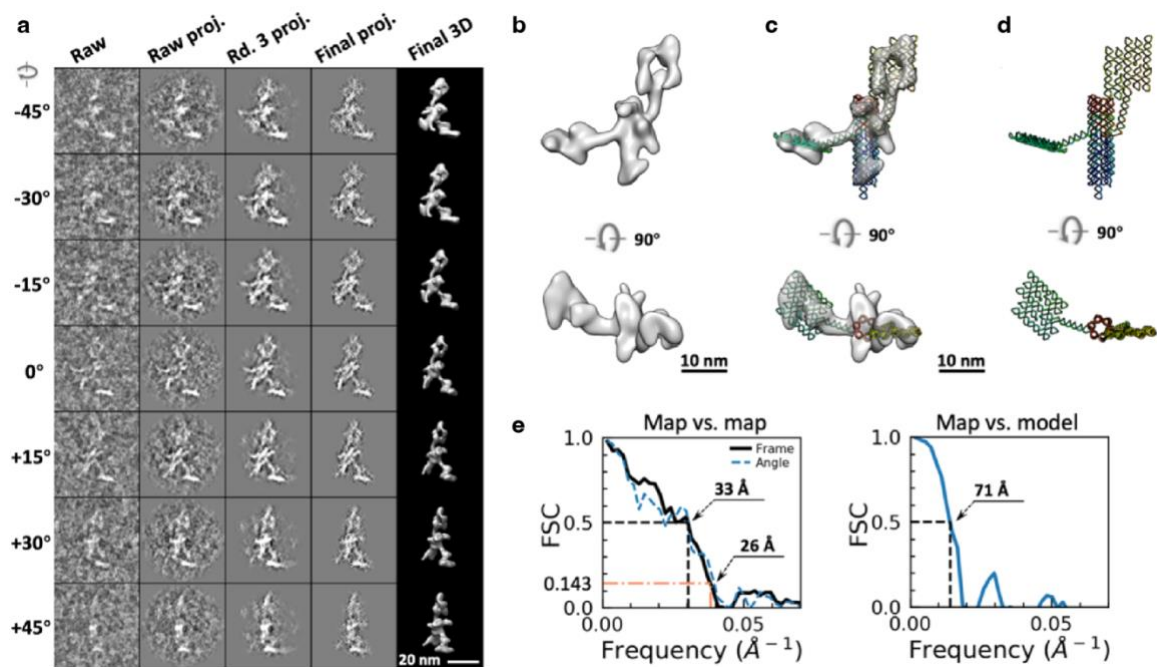
**a**, Seven representative tilt images of a 16HS particle displayed in the first column from the left. Using IPET, the tilt images are aligned to a common center *via* iterative refinements. The projections of raw, intermediate and final 3D reconstructions at the corresponding tilt angles are displayed in the next four columns. **b**, Two perpendicular views of the final 3D density map; **c**, the map superimposed with the flexible docked model; and **d** the fitted model. **e**, FSC analyses of the final map resolution by two methods, the “map vs. map” (the map reconstructed from the half tilt series, such as even index, against that from the other half tilt series) and “map vs. model” (the map against the density map generated from the model). Two resolutions were measured for “map vs. map” at FSC=0.5 and FSC=0.143 and one resolution was measured for “map vs. model” at FSC=0.5.





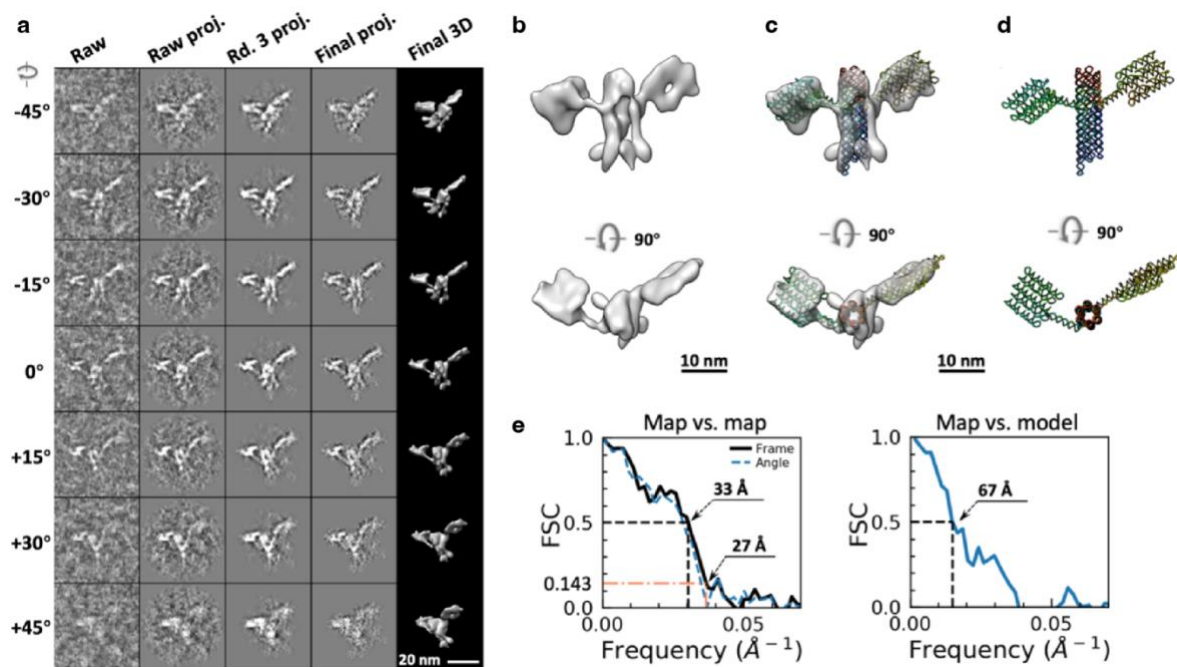
**Supplementary Fig. 19. IPET 3D reconstruction of individual particle #4 of 16HS.**

**a**, Seven representative tilt images of a 16HS particle displayed in the first column from the left. Using IPET, the tilt images are aligned to a common center *via* iterative refinements. The projections of raw, intermediate and final 3D reconstructions at the corresponding tilt angles are displayed in the next four columns. **b**, Two perpendicular views of the final 3D density map; **c**, the map superimposed with the flexible docked model; and **d** the fitted model. **e**, FSC analyses of the final map resolution by two methods, the “map vs. map” (the map reconstructed from the half tilt series, such as even index, against that from the other half tilt series) and “map vs. model” (the map against the density map generated from the model). Two resolutions were measured for “map vs. map” at FSC=0.5 and FSC=0.143 and one resolution was measured for “map vs. model” at FSC=0.5.



**Supplementary Fig. 20. IPET 3D reconstruction of individual particle #5 of 16HS.**

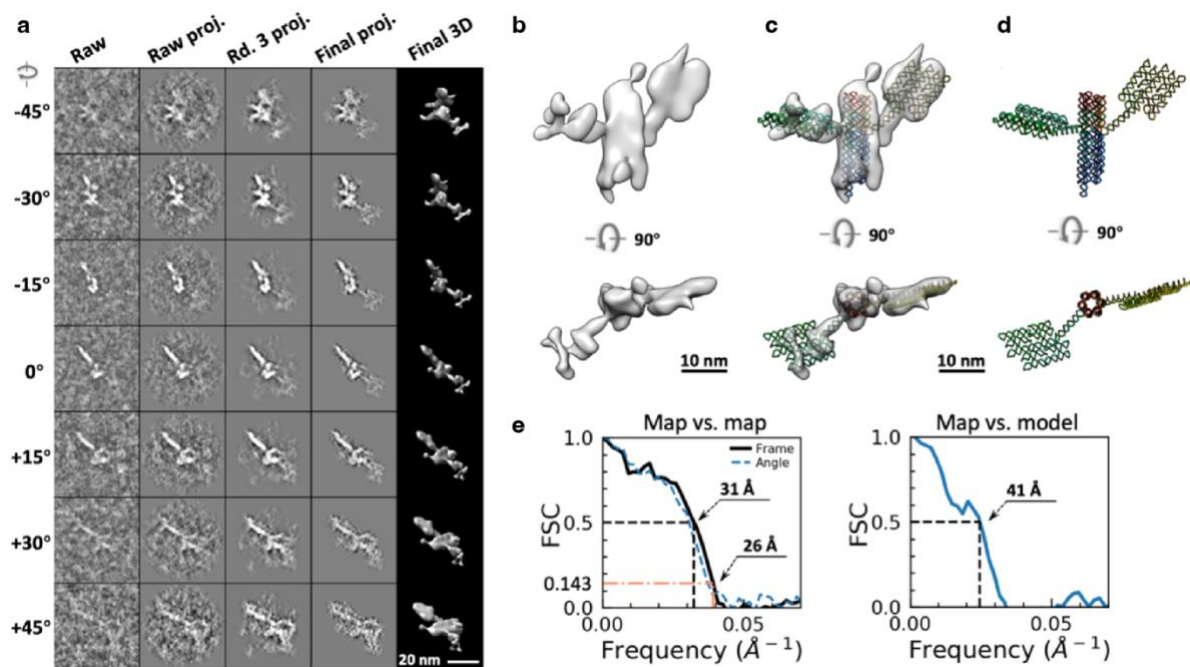
**a**, Seven representative tilt images of a 16HS particle displayed in the first column from the left. Using IPET, the tilt images are aligned to a common center *via* iterative refinements. The projections of raw, intermediate and final 3D reconstructions at the corresponding tilt angles are displayed in the next four columns. **b**, Two perpendicular views of the final 3D density map; **c**, the map superimposed with the flexible docked model; and **d** the fitted model. **e**, FSC analyses of the final map resolution by two methods, the “map vs. map” (the map reconstructed from the half tilt series, such as even index, against that from the other half tilt series) and “map vs. model” (the map against the density map generated from the model). Two resolutions were measured for “map vs. map” at FSC=0.5 and FSC=0.143 and one resolution was measured for “map vs. model” at FSC=0.5.



**Supplementary Fig. 21. IPET 3D reconstruction of individual particle #6 of 16HS.**

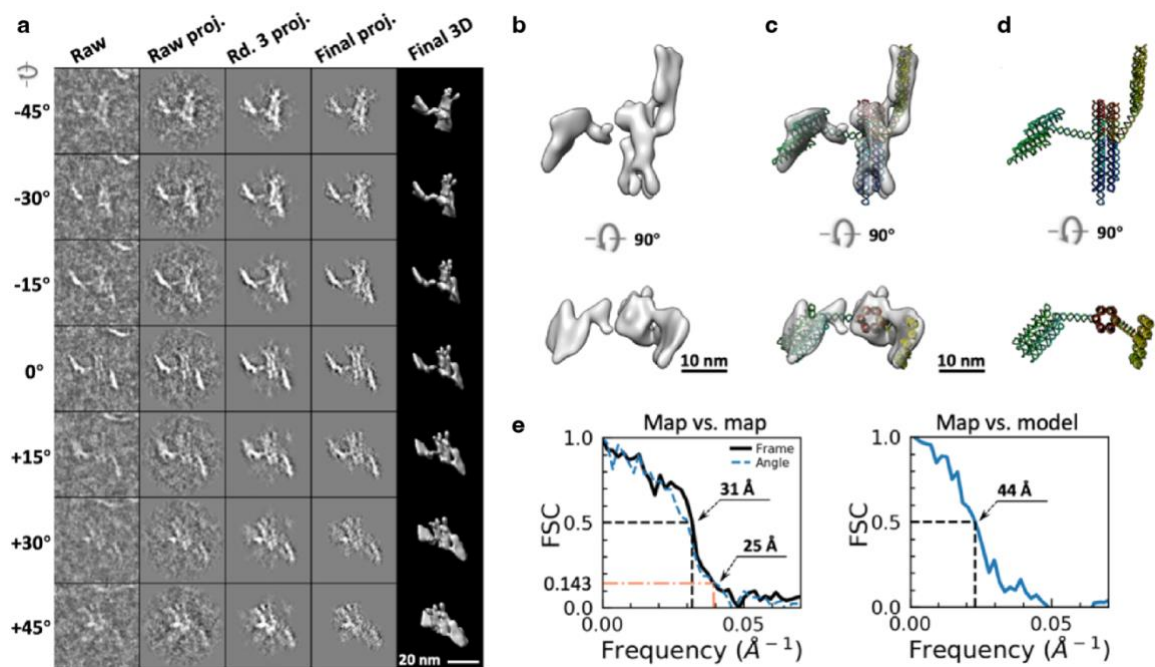
**a**, Seven representative tilt images of a 16HS particle displayed in the first column from the left. Using IPET, the tilt images are aligned to a common center *via* iterative refinements. The projections of raw, intermediate and final 3D reconstructions at the corresponding tilt angles are displayed in the next four columns. **b**, Two perpendicular views of the final 3D density map; **c**, the map superimposed with the flexible docked model; and **d** the fitted model. **e**, FSC analyses of the final map resolution by two methods, the “map vs. map” (the map reconstructed from the half tilt series, such as even index, against that from the other half tilt series) and “map vs. model” (the map against the density map generated from the model). Two resolutions were measured for “map vs. map” at FSC=0.5 and FSC=0.143 and one resolution was measured for “map vs. model” at FSC=0.5.





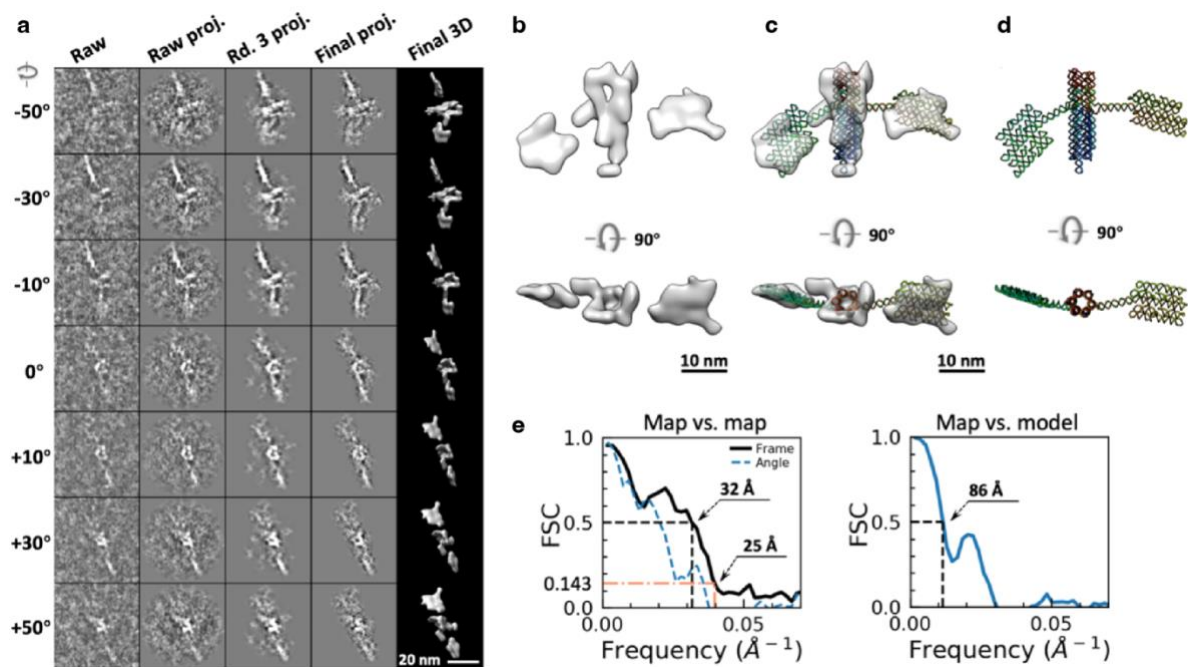
**Supplementary Fig. 22. IPET 3D reconstruction of individual particle #7 of 16HS.**

**a**, Seven representative tilt images of a 16HS particle displayed in the first column from the left. Using IPET, the tilt images are aligned to a common center *via* iterative refinements. The projections of raw, intermediate and final 3D reconstructions at the corresponding tilt angles are displayed in the next four columns. **b**, Two perpendicular views of the final 3D density map; **c**, the map superimposed with the flexible docked model; and **d** the fitted model. **e**, FSC analyses of the final map resolution by two methods, the “map vs. map” (the map reconstructed from the half tilt series, such as even index, against that from the other half tilt series) and “map vs. model” (the map against the density map generated from the model). Two resolutions were measured for “map vs. map” at FSC=0.5 and FSC=0.143 and one resolution was measured for “map vs. model” at FSC=0.5.



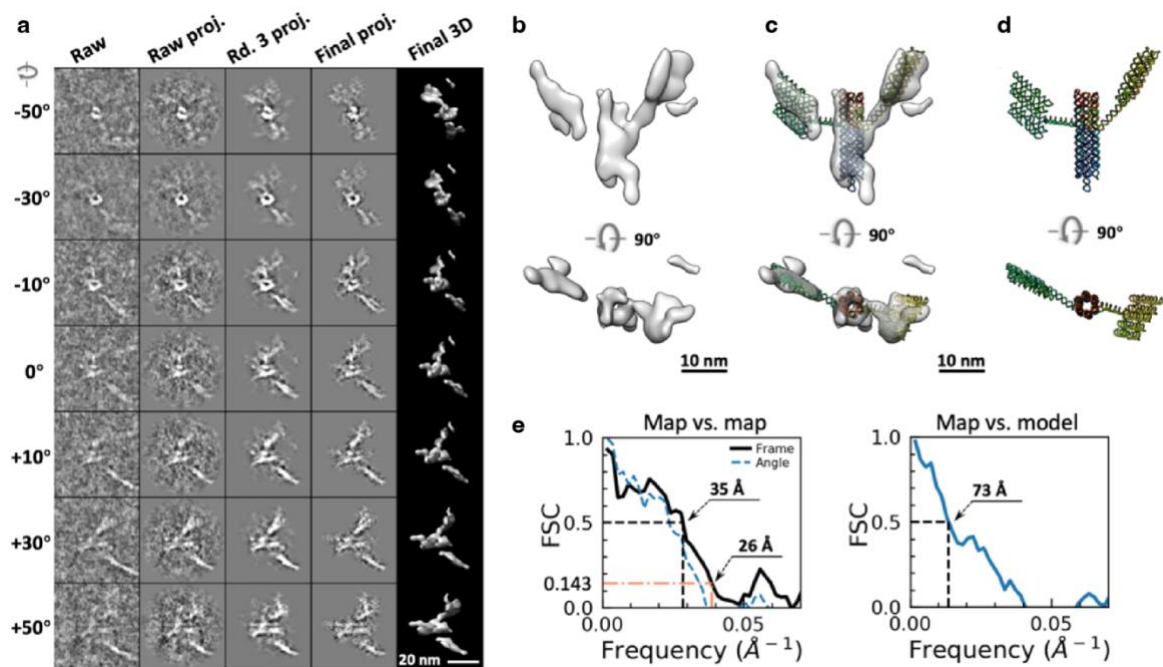
**Supplementary Fig. 23. IPET 3D reconstruction of individual particle #8 of 16HS.**

**a**, Seven representative tilt images of a 16HS particle displayed in the first column from the left. Using IPET, the tilt images are aligned to a common center *via* iterative refinements. The projections of raw, intermediate and final 3D reconstructions at the corresponding tilt angles are displayed in the next four columns. **b**, Two perpendicular views of the final 3D density map; **c**, the map superimposed with the flexible docked model; and **d** the fitted model. **e**, FSC analyses of the final map resolution by two methods, the “map vs. map” (the map reconstructed from the half tilt series, such as even index, against that from the other half tilt series) and “map vs. model” (the map against the density map generated from the model). Two resolutions were measured for “map vs. map” at FSC=0.5 and FSC=0.143 and one resolution was measured for “map vs. model” at FSC=0.5.



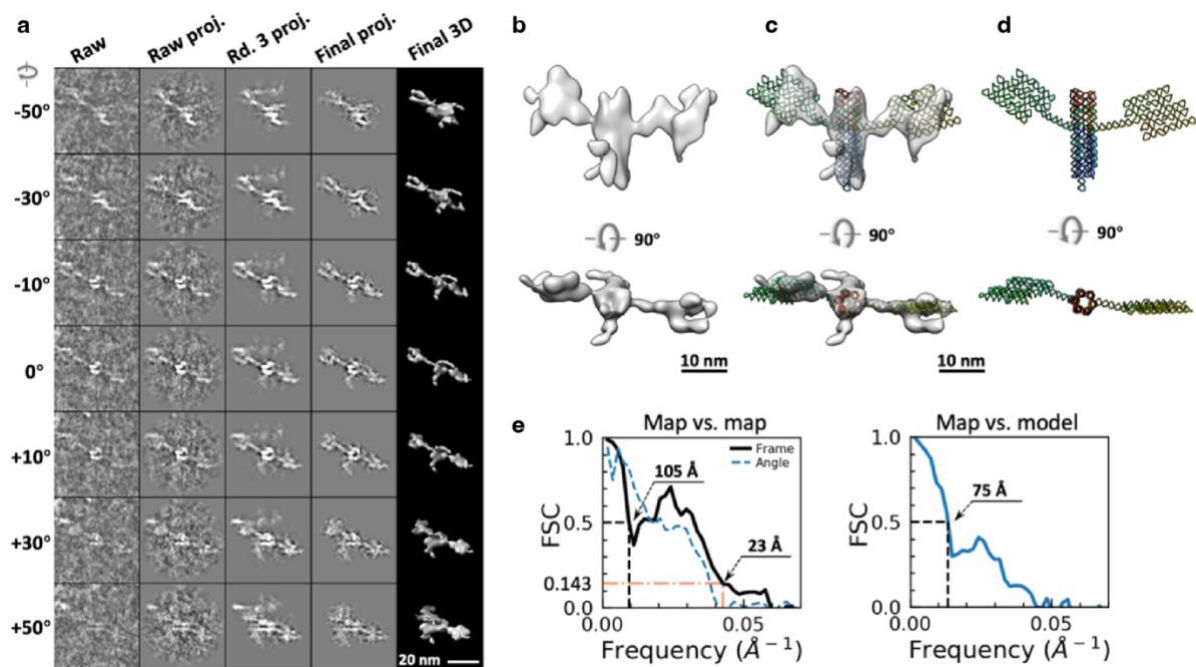
**Supplementary Fig. 24. IPET 3D reconstruction of individual particle #9 of 16HS.**

**a**, Seven representative tilt images of a 16HS particle displayed in the first column from the left. Using IPET, the tilt images are aligned to a common center *via* iterative refinements. The projections of raw, intermediate and final 3D reconstructions at the corresponding tilt angles are displayed in the next four columns. **b**, Two perpendicular views of the final 3D density map; **c**, the map superimposed with the flexible docked model; and **d** the fitted model. **e**, FSC analyses of the final map resolution by two methods, the “map vs. map” (the map reconstructed from the half tilt series, such as even index, against that from the other half tilt series) and “map vs. model” (the map against the density map generated from the model). Two resolutions were measured for “map vs. map” at FSC=0.5 and FSC=0.143 and one resolution was measured for “map vs. model” at FSC=0.5.



**Supplementary Fig. 25. IPET 3D reconstruction of individual particle #10 of 16HS.**

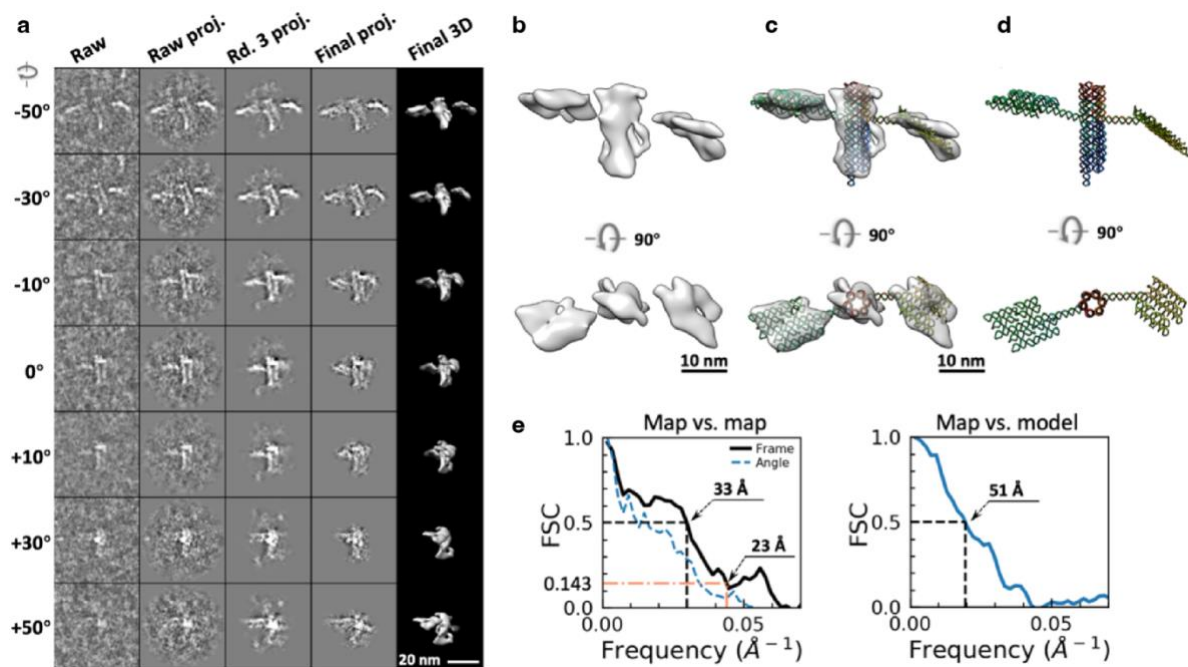
**a**, Seven representative tilt images of a 16HS particle displayed in the first column from the left. Using IPET, the tilt images are aligned to a common center *via* iterative refinements. The projections of raw, intermediate and final 3D reconstructions at the corresponding tilt angles are displayed in the next four columns. **b**, Two perpendicular views of the final 3D density map; **c**, the map superimposed with the flexible docked model; and **d** the fitted model. **e**, FSC analyses of the final map resolution by two methods, the “map vs. map” (the map reconstructed from the half tilt series, such as even index, against that from the other half tilt series) and “map vs. model” (the map against the density map generated from the model). Two resolutions were measured for “map vs. map” at FSC=0.5 and FSC=0.143 and one resolution was measured for “map vs. model” at FSC=0.5.



**Supplementary Fig. 26. IPET 3D reconstruction of individual particle #11 of 16HS.**

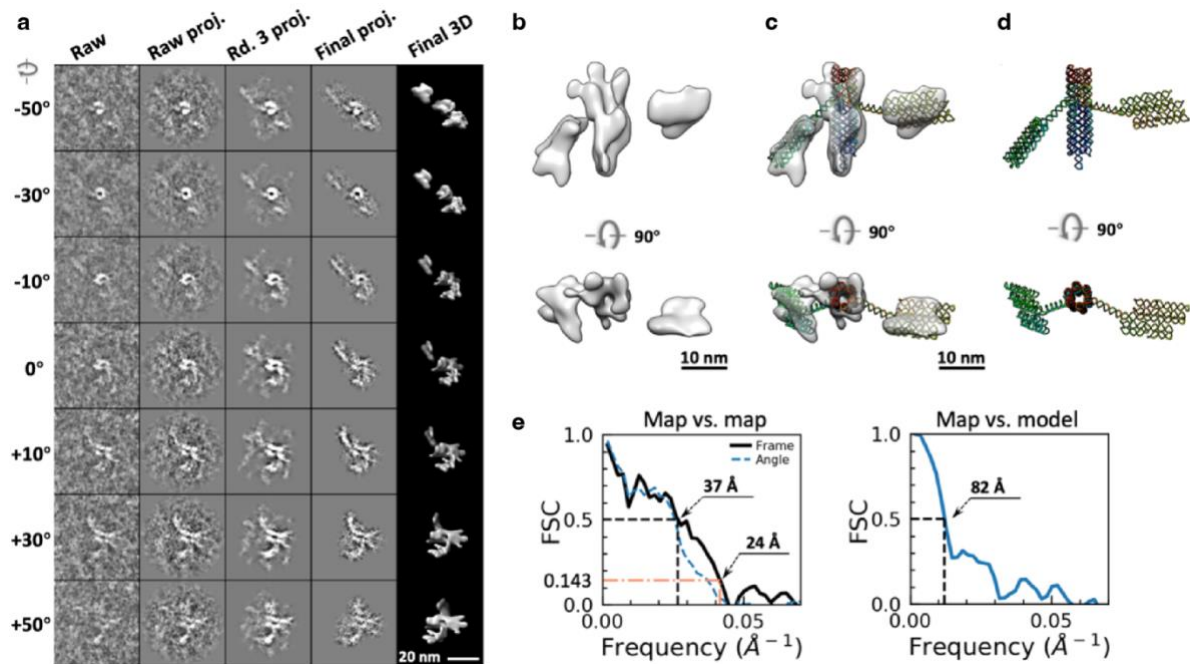
**a**, Seven representative tilt images of a 16HS particle displayed in the first column from the left. Using IPET, the tilt images are aligned to a common center *via* iterative refinements. The projections of raw, intermediate and final 3D reconstructions at the corresponding tilt angles are displayed in the next four columns. **b**, Two perpendicular views of the final 3D density map; **c**, the map superimposed with the flexible docked model; and **d** the fitted model. **e**, FSC analyses of the final map resolution by two methods, the “map vs. map” (the map reconstructed from the half tilt series, such as even index, against that from the other half tilt series) and “map vs. model” (the map against the density map generated from the model). Two resolutions were measured for “map vs. map” at FSC=0.5 and FSC=0.143 and one resolution was measured for “map vs. model” at FSC=0.5.





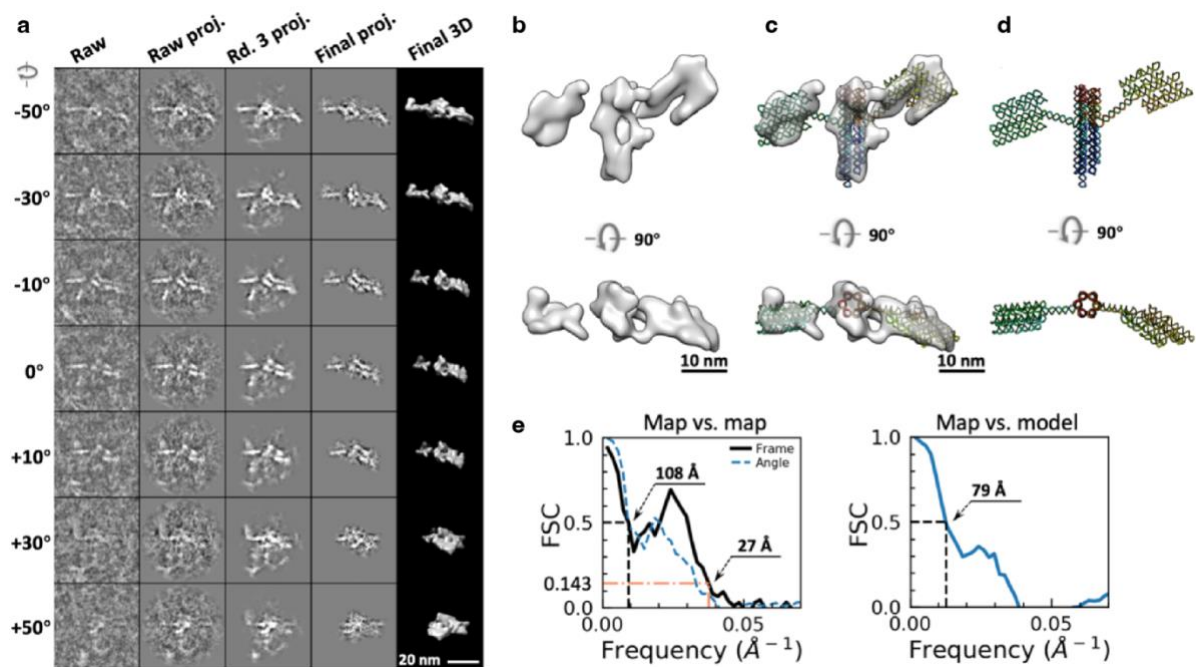
**Supplementary Fig. 27. IPET 3D reconstruction of individual particle #12 of 16HS.**

**a**, Seven representative tilt images of a 16HS particle displayed in the first column from the left. Using IPET, the tilt images are aligned to a common center *via* iterative refinements. The projections of raw, intermediate and final 3D reconstructions at the corresponding tilt angles are displayed in the next four columns. **b**, Two perpendicular views of the final 3D density map; **c**, the map superimposed with the flexible docked model; and **d** the fitted model. **e**, FSC analyses of the final map resolution by two methods, the “map vs. map” (the map reconstructed from the half tilt series, such as even index, against that from the other half tilt series) and “map vs. model” (the map against the density map generated from the model). Two resolutions were measured for “map vs. map” at FSC=0.5 and FSC=0.143 and one resolution was measured for “map vs. model” at FSC=0.5.



**Supplementary Fig. 28. IPET 3D reconstruction of individual particle #13 of 16HS.**

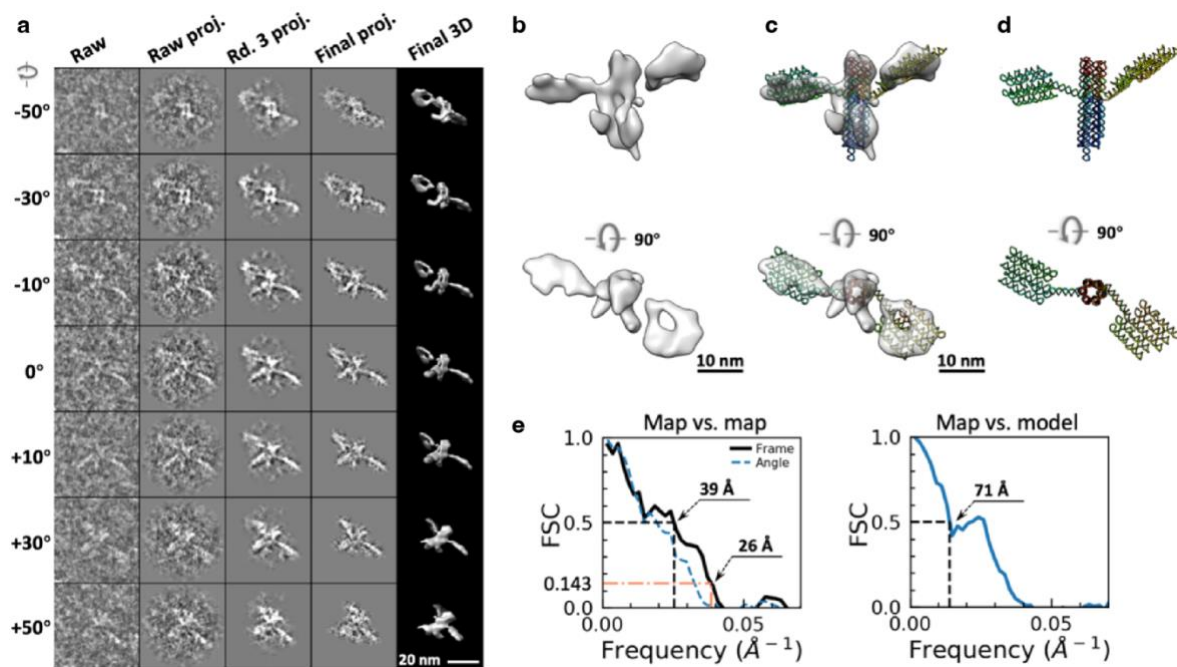
**a**, Seven representative tilt images of a 16HS particle displayed in the first column from the left. Using IPET, the tilt images are aligned to a common center *via* iterative refinements. The projections of raw, intermediate and final 3D reconstructions at the corresponding tilt angles are displayed in the next four columns. **b**, Two perpendicular views of the final 3D density map; **c**, the map superimposed with the flexible docked model; and **d** the fitted model. **e**, FSC analyses of the final map resolution by two methods, the “map vs. map” (the map reconstructed from the half tilt series, such as even index, against that from the other half tilt series) and “map vs. model” (the map against the density map generated from the model). Two resolutions were measured for “map vs. map” at FSC=0.5 and FSC=0.143 and one resolution was measured for “map vs. model” at FSC=0.5.



**Supplementary Fig. 29. IPET 3D reconstruction of individual particle #14 of 16HS.**

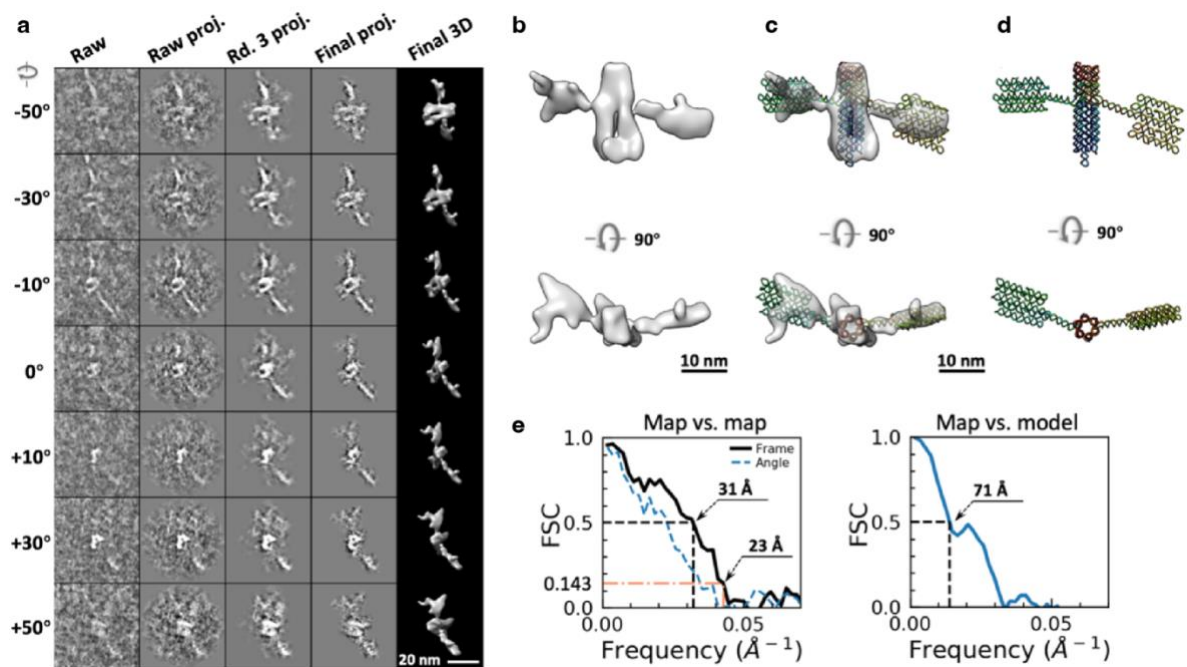
**a**, Seven representative tilt images of a 16HS particle displayed in the first column from the left. Using IPET, the tilt images are aligned to a common center *via* iterative refinements. The projections of raw, intermediate and final 3D reconstructions at the corresponding tilt angles are displayed in the next four columns. **b**, Two perpendicular views of the final 3D density map; **c**, the map superimposed with the flexible docked model; and **d** the fitted model. **e**, FSC analyses of the final map resolution by two methods, the “map vs. map” (the map reconstructed from the half tilt series, such as even index, against that from the other half tilt series) and “map vs. model” (the map against the density map generated from the model). Two resolutions were measured for “map vs. map” at FSC=0.5 and FSC=0.143 and one resolution was measured for “map vs. model” at FSC=0.5.





**Supplementary Fig. 30. IPET 3D reconstruction of individual particle #15 of 16HS.**

**a**, Seven representative tilt images of a 16HS particle displayed in the first column from the left. Using IPET, the tilt images are aligned to a common center *via* iterative refinements. The projections of raw, intermediate and final 3D reconstructions at the corresponding tilt angles are displayed in the next four columns. **b**, Two perpendicular views of the final 3D density map; **c**, the map superimposed with the flexible docked model; and **d** the fitted model. **e**, FSC analyses of the final map resolution by two methods, the “map vs. map” (the map reconstructed from the half tilt series, such as even index, against that from the other half tilt series) and “map vs. model” (the map against the density map generated from the model). Two resolutions were measured for “map vs. map” at FSC=0.5 and FSC=0.143 and one resolution was measured for “map vs. model” at FSC=0.5.



**Supplementary Fig. 31. IPET 3D reconstruction of individual particle #16 of 16HS.**

**a**, Seven representative tilt images of a 16HS particle displayed in the first column from the left. Using IPET, the tilt images are aligned to a common center *via* iterative refinements. The projections of raw, intermediate and final 3D reconstructions at the corresponding tilt angles are displayed in the next four columns. **b**, Two perpendicular views of the final 3D density map; **c**, the map superimposed with the flexible docked model; and **d** the fitted model. **e**, FSC analyses of the final map resolution by two methods, the “map vs. map” (the map reconstructed from the half tilt series, such as even index, against that from the other half tilt series) and “map vs. model” (the map against the density map generated from the model). Two resolutions were measured for “map vs. map” at FSC=0.5 and FSC=0.143 and one resolution was measured for “map vs. model” at FSC=0.5.